© 2015. Published by The Company of Biologists Ltd | Development (2015) 142, 4340-4350 doi:10.1242/dev.125252

RESEARCH ARTICLE

SOX9 modulates the expression of key transcription factors required for heart valve development

Victoria C. Garside[1,2], Rebecca Cullum[1], Olivia Alder[1], Daphne Y. Lu[1], Ryan Vander Werff[3], Mikhail Bilenky[4], Yongjun Zhao[4], Steven J. M. Jones[4,5,6], Marco A. Marra[4,5], T. Michael Underhill[2,3,5] and Pamela A. Hoodless[1,2,5,*]

ABSTRACT

Heart valve formation initiates when endothelial cells of the heart transform into mesenchyme and populate the cardiac cushions. The transcription factor SOX9 is highly expressed in the cardiac cushion mesenchyme, and is essential for heart valve development. Loss of *Sox9* in mouse cardiac cushion mesenchyme alters cell proliferation, embryonic survival, and valve formation. Despite this important role, little is known about how SOX9 regulates heart valve formation or its transcriptional targets. Therefore, we mapped putative SOX9 binding sites by ChIP-Seq in E12.5 heart valves, a stage at which the valve mesenchyme is actively proliferating and initiating differentiation. Embryonic heart valves have been shown to express a high number of genes that are associated with chondrogenesis, including several extracellular matrix proteins and transcription factors that regulate chondrogenesis. Therefore, we compared regions of putative SOX9 DNA binding between E12.5 heart valves and E12.5 limb buds. We identified context-dependent and context-independent SOX9-interacting regions throughout the genome. Analysis of context-independent SOX9 binding suggests an extensive role for SOX9 across tissues in regulating proliferation-associated genes including key components of the AP-1 complex. Integrative analysis of tissue-specific SOX9-interacting regions and gene expression profiles on *Sox9*-deficient heart valves demonstrated that SOX9 controls the expression of several transcription factors with previously identified roles in heart valve development, including *Twist1*, *Sox4*, *Mecom* and *Pitx2*. Together, our data identify SOX9-coordinated transcriptional hierarchies that control cell proliferation and differentiation during valve formation.

KEY WORDS: Transcriptional networks, SOX9, Heart valves, Proliferation, Transcription factor, Limb, ChIP-Seq, Genome, Mouse, Embryogenesis, RNA-Seq

INTRODUCTION

One-third of cardiovascular birth defects are due to abnormal formation of the heart valves and valve insufficiency can lead to increased disease susceptibility later in life. Heart valves develop at two constrictions in the embryonic heart tube: between the atria and ventricles, known as the atrioventricular canal (AVC), and in the outflow tract (OFT), which forms the base of the aorta and pulmonary trunk (reviewed by de Vlaming et al., 2012). These regions form the mitral and tricuspid valves, and aortic and pulmonary valves, respectively (reviewed by Person et al., 2005). Starting at embryonic day (E) 9.5 in the mouse, epithelial-to-mesenchymal transition (EMT) occurs in the endocardial cells of the AVC, in part by responding to the activation of Notch signalling (Timmerman et al., 2004), and leads to their transformation into migratory cells. These cells invade and populate the extracellular matrix (ECM) that separates the endocardium and myocardium to form the cardiac cushions, the precursors of the valves and septa (reviewed by Person et al., 2005). These mesenchymal cells will proliferate, differentiate and remodel to eventually form the mature, thin, delicate valve leaflets (reviewed by de Vlaming et al., 2012).

Transcription factors (TFs) are essential for the precise coordination of lineage specification and differentiation, and ultimately the control of cell identity. In the heart valve, several TFs contribute to this role, but how these TFs are coordinated to regulate valve formation is not known. SOX (SRY-type box) 9, a high mobility group (HMG)-box TF, is highly expressed in the newly formed mesenchyme of the developing heart valves (Montero et al., 2002) and its expression is directly downstream of Notch signalling (Chang et al., 2014). In mouse, SOX9 has an essential role in heart valve development (Lincoln et al., 2007): loss of SOX9 in early valve formation leads to hypoplastic endocardial cushions, reduced proliferation and altered ECM deposition whereas at later stages of valve development, the loss of SOX9 causes abnormal ECM patterning, loss of cartilage-associated proteins, and thickened valves (Lincoln et al., 2007). Lack of SOX9 at either time point in heart valve development is embryonic lethal. In humans, haploinsufficient mutations in the SOX9 locus cause campomelic dysplasia (Wagner et al., 1994), in which there are skeletal abnormalities such as bowing of the long bones, sex reversal, and multiple organ defects, including pancreas and heart defects, that often lead to neonatal death (reviewed by Jain and Sen, 2014).

Embryonic heart valves have been shown to express a high number of genes associated with chondrogenesis, including extracellular matrix protein genes and a number of common key TFs, such as SOX9, TWIST1 and NFATC1 (Chakraborty et al., 2010a). Similar to heart valves, cartilage-containing tissues such as the limb differentiate from SOX9-positive mesenchyme, suggesting that their transcriptional programmes are analogous. During cartilage formation in developing limb buds, loss of SOX9 before mesenchymal condensation leads to cartilage agenesis and subsequent loss of bone formation (Akiyama et al., 2002). Limb buds with SOX9 deletion following the initial formation of cartilage have mesenchymal condensations that are severely hypoplastic and have defects in chondrocyte differentiation and

[1]Terry Fox Laboratory, BC Cancer Agency, Vancouver, Canada V5Z 1L3. [2]Program in Cell and Developmental Biology, University of British Columbia, Vancouver, Canada V6T 1Z4. [3]Biomedical Research Centre, University of British Columbia, Vancouver, Canada V6T 1Z4. [4]Canada's Michael Smith Genome Sciences Centre, BC Cancer Agency, Vancouver, Canada V5Z 1L3. [5]Department of Medical Genetics, University of British Columbia, Vancouver, Canada V6T 1Z4. [6]Department of Molecular Biology and Biochemistry, Simon Fraser University, Burnaby, Canada V5A 1S6.

*Author for correspondence (hoodless@bccrc.ca)

Received 13 April 2015; Accepted 28 October 2015

Development (2015) 142, 4340-4350 doi:10.1242/dev.125252

proliferation (Akiyama et al., 2002). Loss of SOX9 in other organ systems also produces hypoplastic organs and defects in proliferation (Lincoln et al., 2007; Trowe et al., 2010; Rockich et al., 2013).

Despite the essential role of SOX9, its mechanisms of action and its transcriptional targets are not well understood. In adult hair follicle stem cells (HF-SCs), genes bound by SOX9 are required for the cells to maintain stemness via secreted factors in the niche (Kadaja et al., 2014). Recently, the global transcriptional targets of SOX9 in chondrocytes have begun to be explored (Liu and Lefebvre, 2015; Ohba et al., 2015). However, only a limited number of bona fide *in vivo* transcriptional targets of SOX9 have been identified in the embryonic limb (Bell et al., 1997; Bridgewater et al., 1998) and no direct *in vivo* SOX9 transcriptional targets are known in embryonic heart valves.

To explore the *in vivo* functional relevance of SOX9 in valve and limb development, we used chromatin immunoprecipitation coupled with next generation sequencing (ChIP-Seq) to generate genome-wide profiles of putative SOX9 DNA-binding sites in E12.5 mouse embryonic AVC and limb. We identified 2607 and 9092 SOX9 peak regions corresponding to 2453 and 5750 potential target genes in the E12.5 AVC and limb, respectively. SOX9 peaks common across multiple tissues supported a role for SOX9 in regulating cell proliferation and specifically identified AP-1 proteins and other cell cycle regulators as targets of SOX9 interactions. Moreover, in heart valves, we identified a group of essential TFs modulated by SOX9. By comparing these potential gene targets of SOX9 to transcriptional changes identified in RNA-Seq data from *Sox9*-deficient AVCs, we have demonstrated that SOX9 is a necessary upstream regulator required to modulate the expression levels of factors essential for heart valve formation.

RESULTS

SOX9 directly binds thousands of DNA regions in the developing heart and limb

At E12.5, SOX9 is widely expressed in mesenchyme throughout the developing valves (Akiyama et al., 2004) and in the condensing limb mesenchyme (Wheatley et al., 1996). To examine the regulatory role of SOX9 in these tissues, we generated genome-wide ChIP-Seq profiles of SOX9 DNA-binding sites for E12.5 heart valves (AVC) and E12.5 limbs. Subsequent to mapping and compiling of the sequencing reads, potential binding regions of SOX9, referred to as 'peaks', were identified using a false discovery rate (FDR) of 0.01 followed by statistical subtraction of an input DNA control. We identified 2607 and 9092 peaks in the AVC and limb, respectively (Fig. 1A; Tables S2-S4). Peaks of SOX9 interaction in the limb supported previously identified regulatory regions that are bound by SOX9, near to the genes *Col2a1*, *Acan* and *Col11a2* (Bell et al., 1997; Bridgewater et al., 1998; Sekiya et al., 2000) (Fig. S1C). To identify similarities in the SOX9-initiated transcriptional programmes, we compared the SOX9 AVC and limb ChIP-Seq libraries and found 782 SOX9 peaks that were shared (30.0% of E12.5 AVC peaks) (Fig. 1A), confirming that SOX9 has common regulatory roles in valve and limb development. An additional 1825 and 8310 SOX9 peaks were unique in the E12.5 AVC and limb, respectively, indicating that SOX9 also has tissue-specific binding sites.

De novo motif analysis of the SOX9 ChIP-Seq peaks with SeqPos (Liu et al., 2011) generated a SOX monomer and a SOX dimer position weight matrix (PWM) (Fig. 1C) that is similar to the SOX9 JASPAR motif. In sex determination, SOX9 is known to bind as a monomer to a single DNA-binding motif in the regulatory regions of the loci for steroidogenic factor 1 (*Nr5a1*) and anti-Müllerian hormone (*Amh*), whereas genes required for chondrogenesis, such

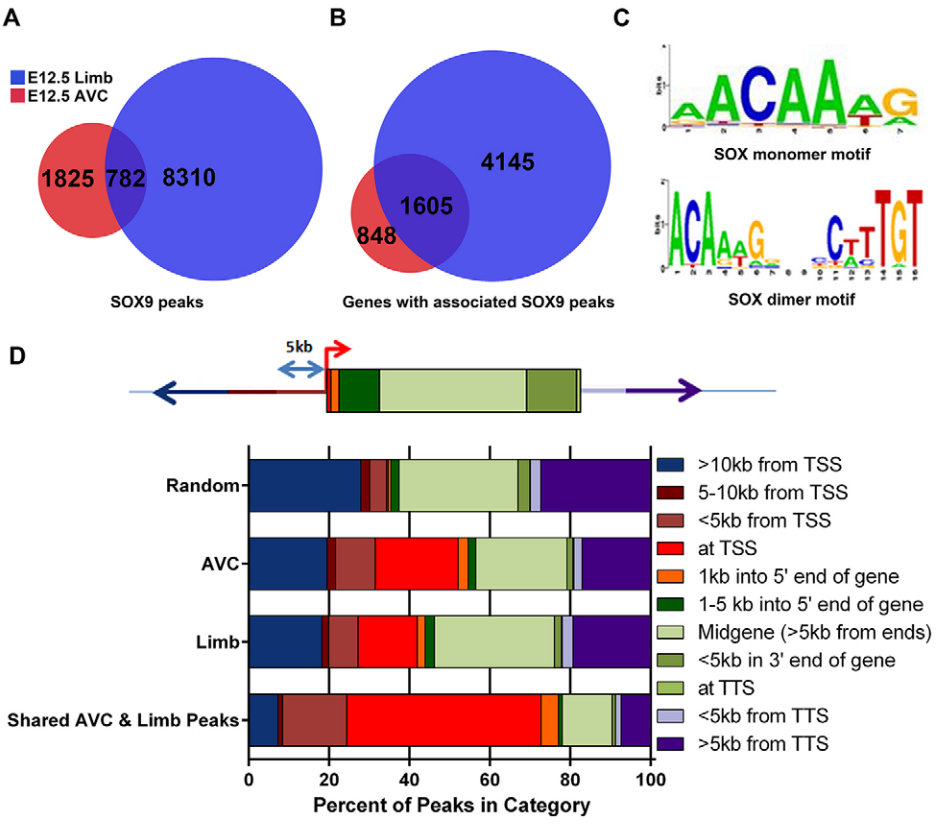

Fig. 1. SOX9 peaks are frequently located in the TSS/promoter in the AVC and limb. (A) Venn diagram of genomic locations of peaks illustrates how many peaks directly overlap between libraries. (B) Venn diagram indicating the genes that are either uniquely targeted or commonly targeted in the E12.5 AVC and limb ChIP-Seq. A gene with an associated SOX9 peak in both tissues may have a peak in the same place in both tissues or at unique tissue-specific regions still targeting the same gene. (C) Positional weight models for the SOX monomer and dimer binding motifs as identified from ChIP-Seq data. Letter height indicates importance of the base for SOX9 binding. (D) Distribution of SOX9 peak locales across the genome in E12.5 AVC, E12.5 limb and shared binding sites.

Development (2015) 142, 4340-4350 doi:10.1242/dev.125252

as *Col10a1* and *Col9a1*, feature two SOX9-binding motifs separated by four nucleotides in reverse and complementary orientation to one another where SOX9 binds as a homodimer (Bernard et al., 2003). This is analogous to the SOX9 dimer motif found in our data. To determine how many SOX9 peaks contain a SOX monomer and/or dimer motif, we scanned all SOX9 peaks with Screen Motif (a tool written by Cliff Meyer and Len Taing in Cistrome; Liu et al., 2011) using the PWMs generated by SeqPos. We found that 77% of SOX9 limb peaks and 58% of SOX9 E12.5 AVC peaks contained at least one monomer or dimer motif (Table S5). In many cases, SOX9 peaks contain multiple SOX9 DNA-binding motifs per peak. The SOX dimer sequence was identified in 34% of SOX9 limb peaks compared with 13.5% of SOX9 AVC peaks, suggesting that SOX9 primarily binds as a monomer in E12.5 heart valves.

SOX9 directly interacts with regulatory regions of genes associated with proliferation

To determine where SOX9 binds in relation to genes, we associated all SOX9 ChIP-Seq peaks to putative target genes through a 'yes-no' process (Fig. S1D; supplementary materials and methods) that categorized where SOX9 peaks are relative to transcriptional start sites (TSSs), intragenic regions or intergenic regions. By weighting associations in this way, SOX9 peaks that localized to intragenic regions were associated with those genes rather than a potentially closer TSS. This mapping system allowed us to associate peaks to genes with fewer potential false positives and ensured that most peaks were only associated with one gene. Approximately 22% and 31% of SOX9 peaks in the limb and AVC, respectively, were located either directly over a TSS or in the 5 kb proximal promoter regions. This is in contrast to the SOX9 family members SOX6, which had only 13.5% of bound sites in TSS and 20 kb upstream regions (An et al., 2011), and SOX3, which had 11% of its bound sites in proximal promoter regions (McAninch and Thomas, 2014). Moreover, a remarkable 63.6% of SOX9 peaks shared between AVC and limb (497 out of 782) were located in the TSS/5 kb promoter regions (Fig. 1D). These data indicate that SOX9 frequently binds to promoters.

We identified 2453 and 5750 genes with associated SOX9 peaks in the E12.5 AVC and limb ChIP-Seq datasets, respectively (Tables S3, S4). Notably, 1605 gene loci that had associated SOX9 peaks were common in both AVC and limb. Of these, 782 SOX9 peaks were overlapping between the two libraries whereas the remaining gene loci had SOX9 peaks associated at different genomic locations in the AVC and limb (Fig. 1B). This suggests that SOX9 interacts with gene loci by using both shared and tissue-specific regulatory elements.

We further delineated common functions of SOX9 by comparing peaks in the AVC and limb with a publicly available SOX9 ChIP-Seq dataset that was generated in mouse HF-SCs (Kadaja et al., 2014) (Fig. 2A). We identified 293 genomic locations with SOX9 peaks in all three ChIP-Seq libraries (Fig. 2A; Fig. S2; Table S6), suggesting that SOX9 occupies analogous regions in mesenchymal tissues and stem cells. Gene Ontology (GO) analysis on the subset of genes associated with these shared SOX9-interacting regions, using the biofunction category (Ingenuity), featured proliferation of cells (Fig. 2B; Table S7). Indeed, 106 of the genes associated with common SOX9 peaks were included in the 'proliferation of cells' category (Table S8). Cell cycle regulators associated with SOX9 peaks in all three libraries include *Junb*, *Cops5*, *Fosl1*, *Fosl2* and *Fos*. Additionally, several genes involved in cell proliferation had SOX9 peaks in heart valve and limb but not HF-SCs (Fig. 2C), such as *Trp53* and *Fgfr2*. ChIP-qPCR on E12.5 AVC and limb further validated the SOX9 ChIP-Seq data, demonstrating that these shared regions were enriched for SOX9 occupancy when compared with IgG (Fig. 2C).

Given that SOX9 is required for the development of many different organs and is known to be involved in progenitor cell proliferation (reviewed by Pritchett et al., 2011), we anticipated that shared SOX9 peaks associated with proliferation genes would also be present in other SOX9-expressing tissues. ChIP-qPCR was performed on the E12.5 lung, gut and liver and demonstrated that many of the shared SOX9 peak regions were also enriched in these tissues (Fig. 2D). Together, our data suggest that analogous SOX9 DNA-binding regions are used in the regulation of cell proliferation across both different cell types and many developing tissues.

SOX9 interacts with regulatory regions for genes crucial for heart valve development

To identify tissue-specific activities of SOX9, we carried out GO analysis on genes associated with SOX9 non-overlapping peaks from each library and filtered out redundant GO terms between each tissue (Fig. 2B; Table S9). HF-SC-specific SOX9-associated genes were enriched for unique GO terms such as stem cell division, hair follicle morphogenesis and cell fate commitment (Fig. 2B). Limb-specific SOX9-associated genes revealed unique GO terms implicated in mesenchyme development, ECM organization and forelimb morphogenesis (Fig. 2B). SOX9 AVC-specific target genes identified unique GO categories involved in DNA binding, cardiac neural crest cell (NCC) development, and ascending aorta morphogenesis. Identifying genes involved in cardiac NCC in the AVC-specific GO categories supports the similarity between AVC and OFT cushion development. Overall, genes associated with tissue-specific SOX9 peaks strongly reflect the unique characteristics of each tissue and this suggests that SOX9 plays a role in, and is strongly linked with, tissue identity.

To parse out crucial transcriptional targets of SOX9 during heart valve development, we took advantage of a mouse model with specific deletion of *Sox9* in which both endocardial cells and newly transformed mesenchymal cells of the developing AVC cushions fail to express SOX9 (Lincoln et al., 2007). These mice have been shown to die during embryogenesis and have heart valve defects including hypoplastic cardiac cushions, reduced mesenchyme proliferation and altered ECM composition. The *Tie2-Cre* mouse, used for this conditional system, has been previously shown to specifically express in endocardial cells and the resulting mesenchymal cells and not cardiomyocytes, epicardium or distal OFT mesenchyme (Kisanuki et al., 2001; Snarr et al., 2008). To ensure deletion of *Sox9* in the E12.5 AVC, immunofluorescence for SOX9 was performed on $Sox9^{fl/fl}$ (wild type; WT) and $Sox9^{fl/fl}$;*Tie2-Cre* (*Sox9* cKO) embryonic hearts (Fig. S3A,B; Fig. S4). As expected, deletion of *Sox9* leads to death in the majority of embryos by E13.5 due to severely hypoplastic and malformed AV valves (Fig. S3A,B; Fig. S4). Additionally, *Sox9* cKO hearts had thinning of the ventricular walls (Fig. S3A, asterisk) and both the atrial and ventricular septums had not fused with the AVC in the *Sox9* cKO compared with WT (Fig. S3A, arrowheads). Illustrating the specificity of *Sox9* deletion with the *Tie2-Cre* lineage, SOX9 expression was lost only in the AVC whereas epicardial cells that descend from a different lineage still express SOX9 (Fig. S3A,B; Fig. S4). A decrease in proliferation in *Sox9* cKO AVCs and AVC explant cultures was also noted (Fig. S5), as seen in previous work (Lincoln et al., 2007).

Development (2015) 142, 4340-4350 doi:10.1242/dev.125252

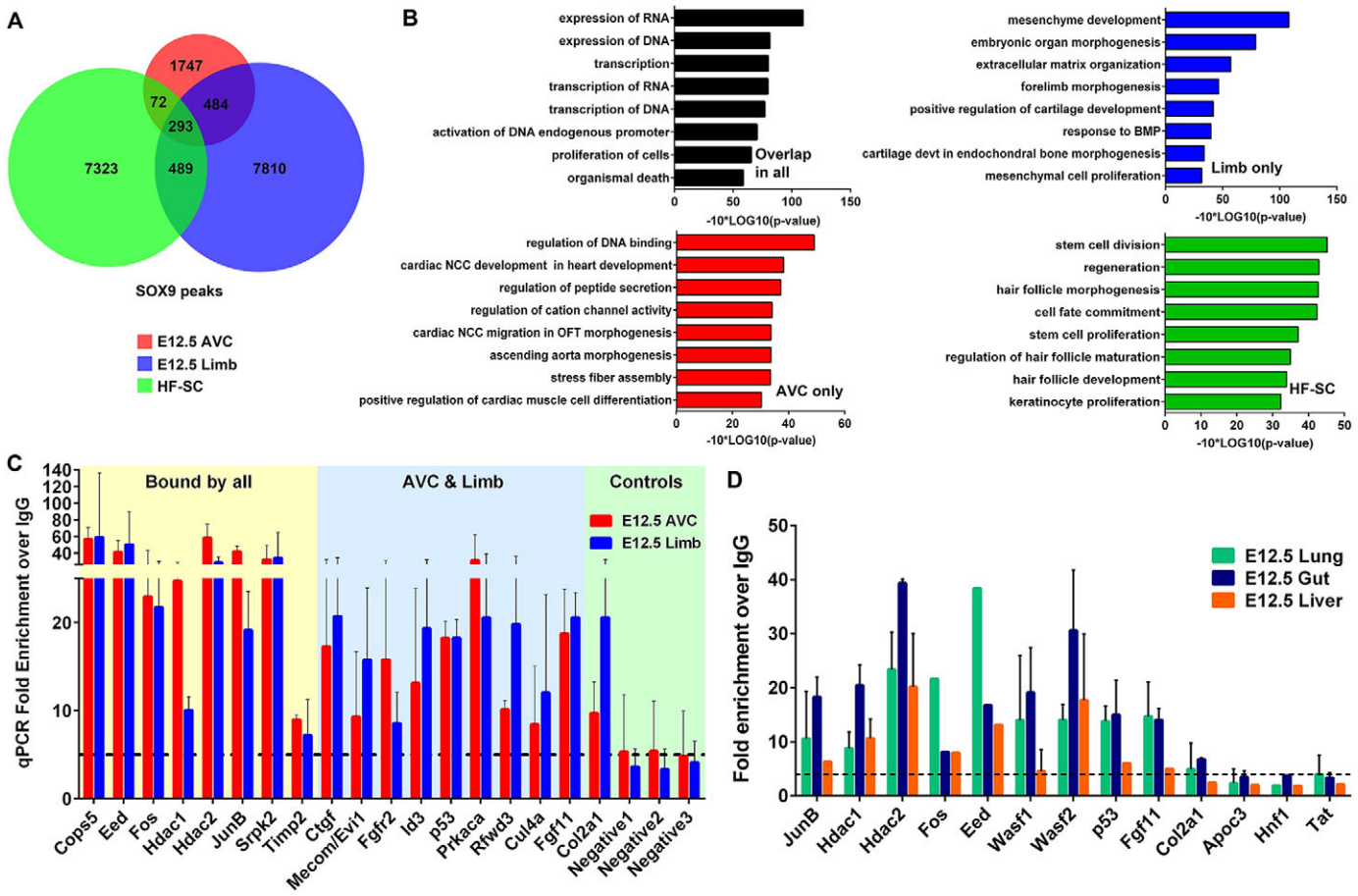

Fig. 2. Genes with associated common SOX9 peaks among developing tissues provide evidence for a mutual role in proliferation. (A) Venn diagram of genomic locations of SOX9 peaks in E12.5 AVC, E12.5 limb, and hair follicle stem cells (HF-SCs). (B) The top eight terms showing enrichment based on *P*-values from GO analysis on the genes associated with the 293 SOX9 overlapping peaks and the genes uniquely associated for each tissue. (C) qPCR showing fold enrichment of SOX9 ChIP over IgG (average and standard deviation of three ChIPs) on the E12.5 AVC and limb validates SOX9 peaks that are common in all three SOX9 ChIP-Seq libraries and associated with genes involved in proliferation of cells. The region previously identified in chondrocytes as a SOX9-bound *Col2a1* enhancer was used as a positive control and unrelated genomic regions were used as negative controls. (D) ChIP-qPCR shows that SOX9 binds to the same regions in E12.5 lung, gut and liver (three ChIPs for *Wasf1/2*, *Hdac1/2*; two ChIPs for *Junb*, *p53*, *Fgf11*, *Col2a1*, *Apoc*, *Tat*; and one ChIP for *Fos* and *Eed*). Standard deviation of ChIP-qPCRs are shown as error bars in C and D. Negative 1, 2, 3 (*Apoc3, Hnf1, Tat*) are negative control regions that do not contain a SOX9 peak. The *Col2a1* regulatory region is a positive control region for SOX9 binding.

To identify downstream mRNA changes resulting from deletion of *Sox9* that might be responsible for the valve defects, we compared the transcriptome of the E12.5 AVC in WT with that of *Sox9* cKO. Because the efficiency of *Sox9* deletion in the AVC by *Tie2-Cre* is variable, RNA was isolated from individual AVCs from E12.5 WT and *Sox9* cKO, and qRT-PCR verified the loss of *Sox9* transcript prior to pooling of two to three AVCs for RNA-Seq libraries. Duplicate libraries were created for each genotype (Fig. S6). Upon comparison, 634 genes were downregulated in the *Sox9* cKO at least 1.5-fold and 610 genes were upregulated in the *Sox9* cKO at least 1.5-fold (Tables S10, S11). Interestingly, downregulated genes in the *Sox9* cKO AVC were categorized by GO as involved in cartilage development, mesenchyme differentiation and EMT (Fig. 3A). Upregulated genes in the *Sox9* cKO included functions such as response to oxidative stress, gas transport and positive regulation of heart rate (Fig. 3B).

To further investigate genes that might be directly regulated by SOX9, we focused on the 145 genes that had both altered expression in AVCs lacking *Sox9* and had an E12.5 AVC SOX9 peak associated. Of these 145 genes, for simplicity referred to as SOX9 target genes, ~60% were downregulated and 40% were upregulated (Tables 1, 2; Table S12). Analysis of the up- and downregulated SOX9 target genes by Ingenuity Pathway Analysis highlighted enrichment in functions associated with transcription and cardiogenesis. Moreover, several of these genes have been linked to abnormal heart morphogenesis (Fig. 3C). Notable target TFs categorized as having roles in heart development that were downregulated in *Sox9* cKO include *Sox4*, *Hand2*, *Twist1*, *Foxp4*, *Mecom* (also known as *Evi1*) and *Pitx2*; upregulated target genes also contained several TFs, such as *Bhlhe40*, *Ddit3* and *Junb* (Tables 1, 2; Table S12). In addition, several ECM components, such as periostin and elastin, were reduced (Table 1; Table S12). Thus, our data suggest that SOX9 can act as a transcriptional activator and repressor. Moreover, our data support a direct role for SOX9 in regulating a network of TFs and ECM components that function during heart valve development.

SOX9 modulates a core network of TFs during heart valve development

Comparison of E12.5 AVC SOX9 ChIP-Seq and RNA-Seq data from *Sox9* deficient valves suggests that SOX9 lies upstream of a network of TFs in developing heart valves. We confirmed reduced

Development (2015) 142, 4340-4350 doi:10.1242/dev.125252

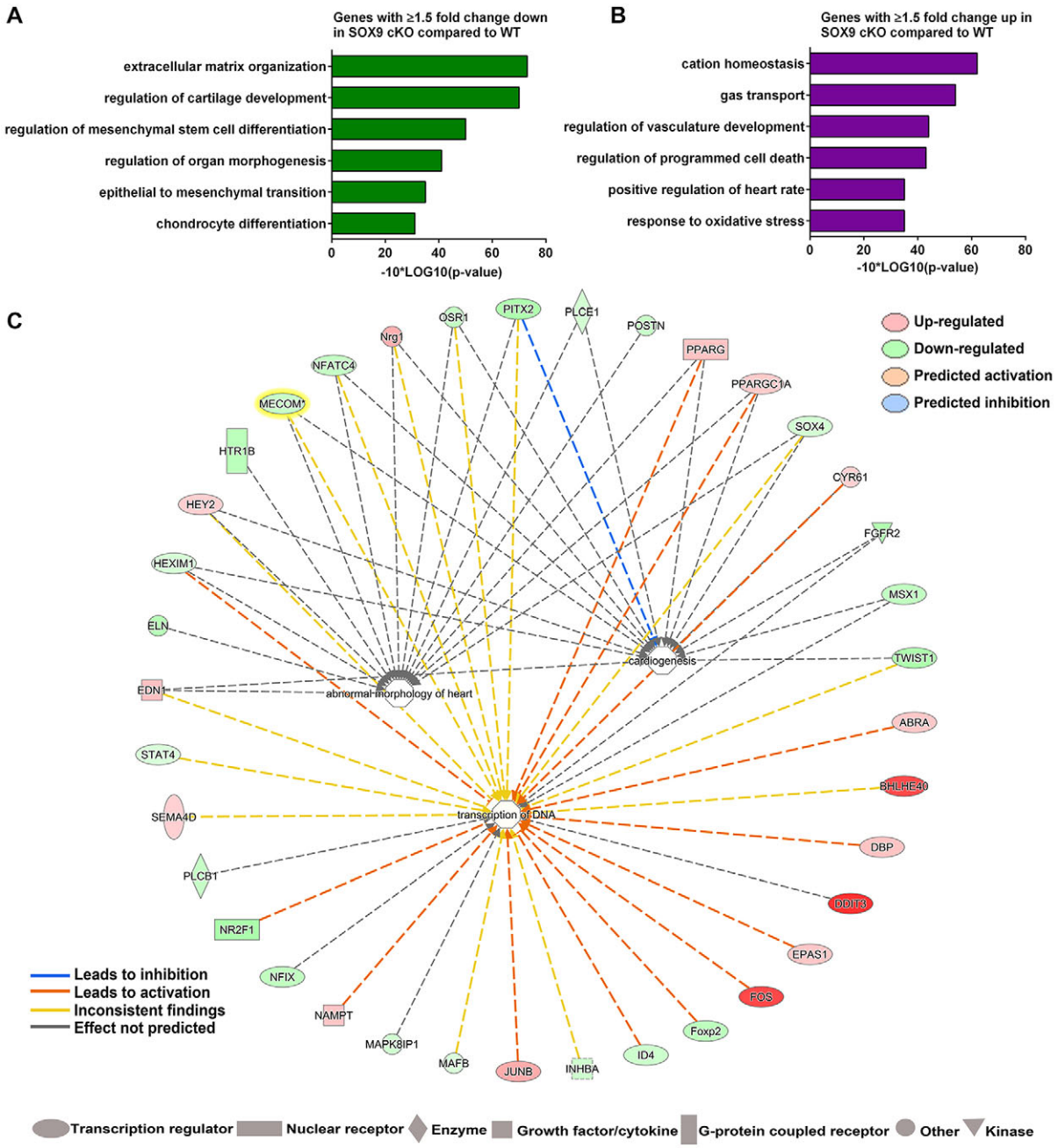

Fig. 3. Comparison of SOX9 ChIP-Seq and differential transcripts in the *Sox9* cKO AVC reveals critical genes involved in valve formation. (A,B) GO analysis on 634 genes down- (A) and 610 upregulated (B) genes with ≥1.5-fold change in E12.5 *Sox9* cKO. (C) Ingenuity identifies a network including biofunctions for transcription of DNA, cardiogenesis and abnormal heart morphology on up- and downregulated genes that have an associated SOX9 peak. Lines indicate the type of relationship between the gene and GO term. For example, loss of *Pitx2* leads to an inhibition of cardiogenesis and both activation and inhibition of transcription of DNA. Yellow lines indicate that there is data to support both activation and inhibition. Libraries were created in duplicate from pooled valves.

mRNA expression in *Sox9* cKO AVC by qRT-PCR of the following TFs: *Sox4*, *Mecom*, *Twist1*, *Pitx2*, *Hand2* and *Nfia* (Fig. 4A). In all cases, mRNA expression of these TFs was substantially reduced in *Sox9* cKO AVCs. Two additional TFs associated with SOX9 peaks that are important in heart valve development, *Lef1* and *Tbx20*, were also significantly reduced in *Sox9* cKO AVC as shown by qRT-PCR (Fig. 4A) but were below the 1.5-fold change cut-off used for the RNA-Seq analysis (*Tbx20*=1.33, *Lef1*=1.29; Table S11). Of note, the two most downregulated (*Btn1a1* and *Prelp*) and two of the most upregulated genes (*Bhlhle40* and *Fos*) in the *Sox9* cKO AVC also associated with SOX9 peaks were confirmed by qRT-PCR (Fig. 4B). Interestingly, little is known about the exact role of these factors during heart valve development.

To confirm that SOX9 can act as a transcriptional activator and repressor, SOX9 peak regions associated with *Mecom*, *Nfia* and *Junb* were cloned into luciferase reporter vectors and, together with SOX9 ectopic expression (pcDNA3-SOX9), luciferase activity was assayed in HEK293T cells (Fig. 4C). *Mecom*- and *Nfia*-associated SOX9 peaks were upstream of the genes in putative enhancers, whereas the SOX9 peak for *Junb* was located within the promoter.

Development (2015) 142, 4340-4350 doi:10.1242/dev.125252

Table 1. The top 20 direct targets of SOX9 with ≥1.5 fold change (FC) down in the *Sox9* cKO AVC

Gene	WT normalized FPKM	*Sox9* cKO normalized FPKM	Log2FC
Btn1a1	14.94	0.58	−3.66
Prelp	7.34	0.77	−2.47
Ctnna2	7.26	1.44	−1.87
1700084E18Rik	4.55	0.86	−1.75
Scrg1	2.15	0.22	−1.72
Gm7244	1.64	0.20	−1.45
Ntn4	19.89	6.48	−1.43
Col6a6	8.50	2.62	−1.41
Lrrn1	2.30	0.47	−1.38
Ptx3	18.61	6.34	−1.37
Nr2f1	17.85	6.11	−1.36
Twist1	75.70	27.94	−1.31
Pitx2	42.88	15.99	−1.28
Eya4	5.92	1.95	−1.27
Fgfr2	44.08	16.70	−1.26
Lmo3	2.48	0.66	−1.23
Thsd7b	11.80	4.41	−1.21
Dlg2	16.87	6.62	−1.17
Eln	59.90	24.51	−1.16
Kctd14	2.20	0.65	−1.11

Mecom has been shown to be expressed in the developing heart valves (Hoyt et al., 1997; Bard-Chapeau et al., 2014) but its exact role in the AV valves is not well understood. NFI factors have been shown to work together with SOX9 to regulate downstream target genes in other systems (Nagy et al., 2011; Kang et al., 2012) and *Junb* has a well-established role in regulating cell cycle. SOX9 ectopic expression activated the *Mecom* and *Nfia* enhancers by 2.45- and 2.37-fold, respectively, whereas SOX9 inhibited the activity of the *Junb* promoter by 1.5-fold (Fig. 4C). These data support the proposal that SOX9 can function to both activate and repress transcription.

The putative enhancer for *Mecom* contains both a SOX9 dimer motif and several monomer motifs. To show that these SOX9 motifs are required for SOX9 regulation of this enhancer, we generated two mutant versions: one with a mutated SOX9 dimer motif (DM) and one with the dimer and monomer motifs mutated (Fig. S7). Deletion of the SOX9 dimer motif resulted in a substantial loss of SOX9-dependent luciferase activity from the *Mecom* enhancer, and mutation of all potential SOX9 motifs led to a complete loss of SOX9-dependent activity (Fig. 4D). These data suggest that the SOX9 dimer motif in the *Mecom* enhancer is essential for the majority of SOX9-dependent induction.

Table 2. The top 20 direct targets of SOX9 with ≥1.5-fold change (FC) up in the *Sox9* cKO AVC

Gene	WT normalized FPKM	*Sox9* cKO normalized FPKM	Log2FC
Ddit3	26.16	154.32	2.64
Fos	5.71	29.13	2.34
Bhlhe40	26.35	123.24	2.31
Adamts18	0.36	2.09	1.57
Gm14005	2.52	7.1	1.4
Dusp4	19.32	45.58	1.32
Stc1	9.93	22.29	1.23
Gm1631/*Platr26*	0.92	2.67	1.19
Junb	4.65	9.53	1.05
Adhfe1	0.71	1.94	1.04
Nrg1	7.1	13.7	0.99
Tom1	0.29	0.94	0.86
Steap1	1.42	2.83	0.86
6430411K18Rik	5.67	9.97	0.86
1700026D08Rik	2.52	4.66	0.85
Adamtsl3	1.41	2.76	0.83
Nrn1	7.68	13	0.82
4831440E17Rik	1.11	2.19	0.79
Gramd1b	22.38	35.93	0.78
Edn1	15.69	25.3	0.78

TWIST1 is highly expressed during the formation of the cardiac cushion mesenchyme and plays important roles in valve mesenchyme proliferation and differentiation (Shelton and Yutzey, 2008; Chakraborty et al., 2010b). Owing to the key role of TWIST1 in heart valve development, we focused on characterizing the transcript levels of *Twist1* in the *Sox9* cKO valves. qRT-PCR confirmed that the *Twist1* transcript is not only reduced at E12.5, as discussed, but also reduced at an earlier time point (E10.5) in the *Sox9* cKO AVC (Fig. S8). Using *in situ* hybridization, we found that *Twist1* mRNA was specifically expressed in the valve mesenchyme in the E12.5 AVC (Fig. 4E; Fig. S9). Although precise quantitative analysis by *in situ* hybridization is not possible, *Twist1* mRNA showed a similar level of reduction as the qRT-PCR in *Sox9* cKO mutant valves at E12.5 (Fig. 4A). Despite the *in vivo* reduction of *Twist1* expression in *Sox9*-deficient AVCs, the *Twist1*-associated enhancer is highly active without SOX9 overexpression using luciferase assays (data not shown). Motif analysis on the *Twist1*-associated enhancer identified a centrally located NF-Y motif and recent work suggests that NF-Y might recruit SOX9 (Shi et al., 2015).

Overall, the identification of SOX9 ChIP-Seq peaks in the E12.5 AVC, and alterations in mRNA levels between WT and *Sox9* cKO AVCs support a model in which SOX9 functions to both activate and repress transcription during heart valve development. SOX9 plays an important role in regulating heart valve-specific regulatory networks by directly activating transcription factors such as *Mecom* and *Nfia*. However, SOX9 might also indirectly regulate factors like *Twist1* via interactions with NF-Y or additional binding partners.

DISCUSSION

During heart valve development, SOX9 is highly expressed in the mesenchyme of the cardiac cushions of the AVC and OFT (Akiyama et al., 2004). Despite the important role of SOX9 in heart valve development, little is known about its mechanisms or the genes regulated by SOX9. Our study has suggested a dual role for SOX9 in the AVC by regulating proliferation of the mesenchyme cells and by modulating key transcription factors that function during heart valve development. To date, our study is the only one to examine SOX9 genomic interactions in embryonic heart and limb tissues.

SOX9 directly interacts with genomic regions of proliferation genes

In this study, we identified 2607 SOX9 ChIP-Seq peaks in the AVC of E12.5 embryonic heart. Owing to reported similarities in gene expression between valve formation and chondrogenesis (reviewed by Lincoln et al., 2006), and the key role of SOX9 in chondrogenesis (Akiyama et al., 2002), we generated and identified 9092 SOX9 ChIP-Seq peaks in E12.5 limb. Recent studies have similarly identified several thousand ChIP-Seq peaks for SOX9, including >27,000 in neonatal rib chrondrocytes (Ohba et al., 2015) and 8177 in HF-SCs (Kadaja et al., 2014).

Development (2015) 142, 4340-4350 doi:10.1242/dev.125252

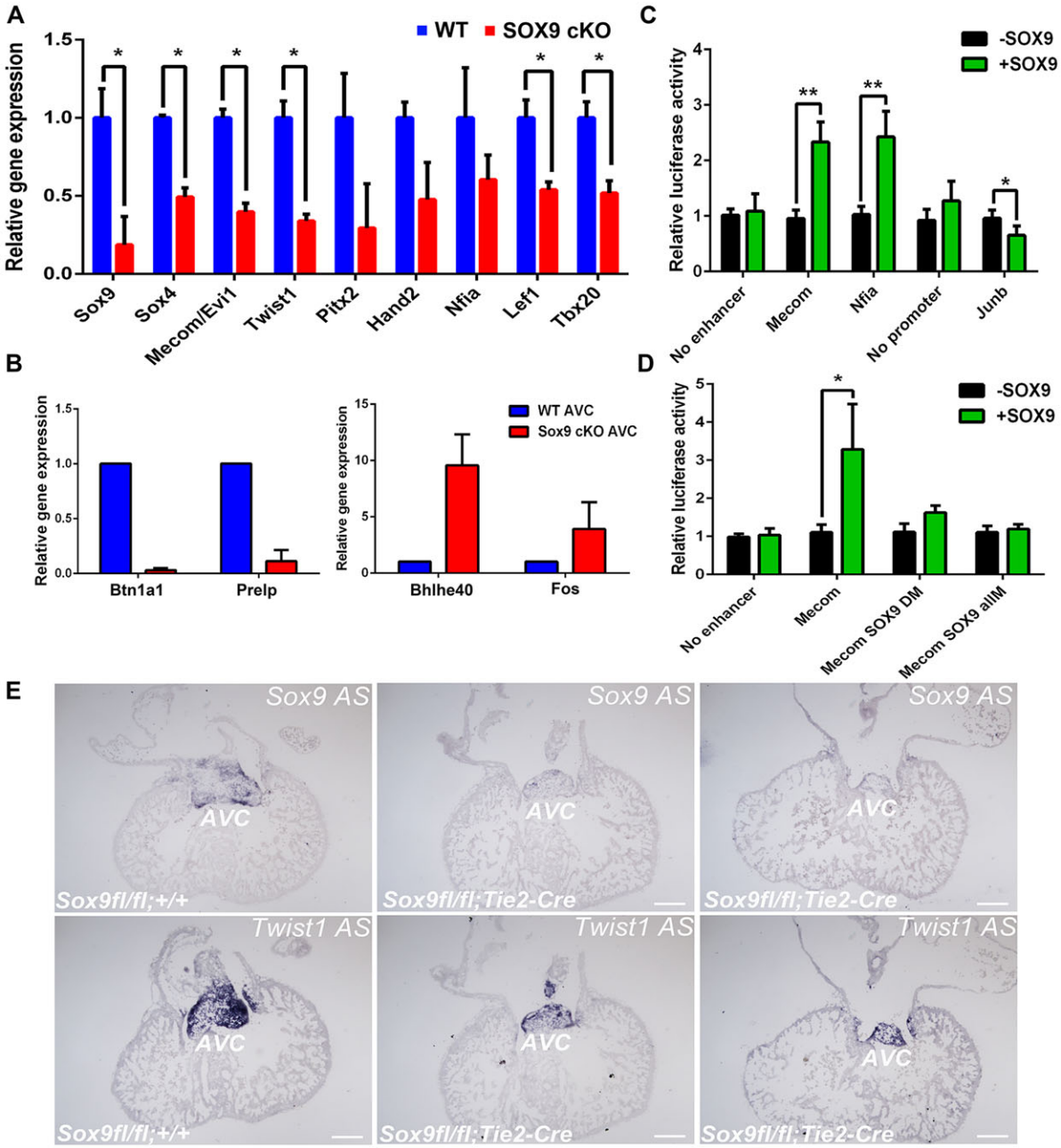

Fig. 4. SOX9 regulates a network of TFs during valve development. (A) qRT-PCR for mRNA expression of *Sox9* and selected target TFs in E12.5 WT and *Sox9* cKO AVCs. (*n*=8+ for *Sox9*, *Twist1*, *Lef1*, *Tbx20*; *n*=3+ for *Sox4*, *Mecom*, *Pitx2*, *Hand2*, *Nfia*). Error bars represent s.e.m. Relative quantification was performed with *Actb* for qRT-PCR or with *Gapdh* for Taqman assays as control. (B) qRT-PCR on the top two down- and upregulated genes that also have associated SOX9 peaks (*n*=2). (C) Luciferase assays on HEK293T cells coupled with/without SOX9 overexpression using regulatory regions identified by SOX9 ChIP-Seq peaks for *Mecom* (enhancer), *Nfia* (enhancer) or *Junb* (promoter). $n \geq 3$. (D) Luciferase assays with site-directed mutagenesis for the *Mecom* enhancer. The *Mecom* enhancer region contained both a dimer and a monomer SOX9 motif and sites were mutated for either just the dimer site (DM) or all sites (allM). $n \geq 3$. (E) *In situ* hybridization for *Sox9* and *Twist1* on E12.5 WT (*Sox9*$^{fl/fl}$;+/+) and *Sox9* cKO (*Sox9*$^{fl/fl}$;*Tie2-Cre*/+) hearts. AS, antisense digoxigenin-labelled probe. **P*<0.05, ***P*<0.01, determined with *t*-tests using the Sidak-Bonferroni method. Error bars represent standard deviation (s.d.) unless otherwise stated. Scale bars: 200 µm.

The relatively lower number of SOX9 peaks observed in the E12.5 AVC is potentially due to the limited amount of chromatin obtained from embryonic heart valves. Alternatively, it might reflect a more restricted role for SOX9 or less heterogeneity in the AVC at this time point. Remarkably, the overlap of SOX9 peaks between AVC, limb bud and HF-SCs is <2% of the total peaks, suggesting that SOX9-interacting regions are numerous and dynamic between tissues. Thus, these studies combine to illustrate the broad diversity of genomic regions that can interact with SOX9, either directly with the DNA or indirectly though other factors.

Although many SOX9 peaks do not overlap, we identified nearly 300 context-independent SOX9 peaks that are located at analogous genomic regions in the three different tissues examined. Many of these shared SOX9 peaks are associated with genes that function in proliferation, which supports a common function of SOX9 in

Development (2015) 142, 4340-4350 doi:10.1242/dev.125252

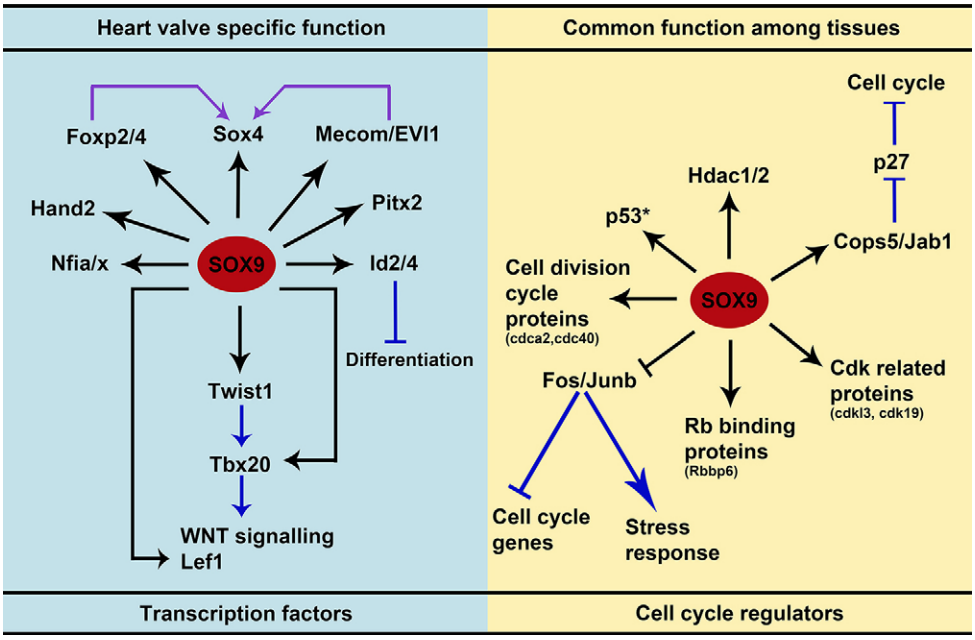

Fig. 5. Model of regulation by SOX9 of heart-specific and common transcriptional networks. Black arrows indicate interactions demonstrated by our data and blue arrows specify previously published data. Purple arrows represent indirect links between molecules. *Note that p53 is targeted by SOX9 in the AVC and limb only and not in HF-SCs.

maintaining a proliferative state during embryonic development (Fig. 5). It has long been known that SOX9 is linked with proliferation. However, a direct mechanistic connection and the transcriptional targets of SOX9 involved in proliferation have remained elusive. In AVC, limb and HF-SCs, SOX9 peaks are associated with three Fos transforming protein family members, *Fos*, *Fosl1* and *Fosl2*. FOS and JUN family members heterodimerize to form the AP-1 complex, which is known to regulate cell proliferation and survival, in part via cyclin D1 expression (Shaulian, 2010). In mesenchymal stem cells, a stable SOX9 knockdown caused reduced proliferation, delayed S-phase progression, and increased cyclin D1 protein stability (Stockl et al., 2013). Of note, *Junb* also has an associated SOX9 peak. Although highly context dependent, JUNB is best known to inhibit cell growth by antagonizing JUN activity (Shaulian, 2010). We show that *Fos* and *Junb* expression is upregulated in SOX9-deficient AVCs, suggesting that their increased expression could contribute to tissue hypoplasia.

In addition to AP-1 complex factors, several genes with roles in cell proliferation have SOX9 peaks in their promoters or potential regulatory regions, including *Cops5*, *Srpk2*, *Akt2*, *Eed*, *Hdac1*, *Hdac2*, *p53* (*Trp53*) and *Prkaca* (PKA). COPS5 (COP9 signalosome subunit 5) associates with JUN proteins to increase binding specificity and can degrade the cell cycle inhibitor p27Kip1 (Cdkn1b) (Claret et al., 1996). Loss of *Cops5* in embryonic limb results in shortened limbs due to impaired chondrogenesis and *Sox9* levels are decreased in mutant long bones (Bashur et al., 2014) suggesting a potential feedback loop between SOX9 and COPS5. SRPK2 (SRSF protein kinase 2) can promote proliferation and cell cycle progression by enhancing cyclin D1 levels (Jang et al., 2009), and AKT2 regulates progression of cell cycle via phosphorylation of its targets including cyclin-dependent kinase inhibitors and maintaining protein stability of MYC and D-type cyclins via GSK3β (Xu et al., 2012). EED (embryonic ectoderm development), HDAC1 and HDAC2 (histone deacetylase 1 and 2) are epigenetic regulators associated with cell proliferation (Bracken et al., 2003; Kelly and Cowley, 2013). p53 activates DNA repair and arrests proliferation by pausing the cell cycle. If the DNA damage is severe, p53 initiates cell death (Giono and Manfredi, 2006). PKA (protein kinase A) is induced by cyclic adenosine monophosphate and regulates cellular growth and proliferation through a variety of mechanisms (Stork and Schmitt, 2002). Of note, PKA phosphorylates SOX9 and increases its activity during chondrogenesis (Huang et al., 2000). The activities of p53 and PKA in cell proliferation might be specific to mesenchyme as SOX9 peaks are found in AVC and limb but not HF-SCs.

Taken together, our data suggest a model in which SOX9 promotes proliferation across multiple cell types during development, including heart valves, by interacting with promoters or enhancers of genes encoding proliferative factors such as AP-1 proteins, kinases, and histone modifiers. As many of these genes are misregulated in a diverse range of diseases, identification of the nature of SOX9 interactions with the regulatory regions of these genes could help to elucidate how regulation of these genes is controlled.

SOX9 modulates the transcript levels of key TFs in heart valve development

Previous work demonstrated that *Sox9* deletion using *Tie2-Cre* is embryonic lethal with hypoplastic cardiac cushions, decreased mesenchyme proliferation and altered ECM (Lincoln et al., 2007). Despite this crucial role of SOX9 in valve development, a very limited number of genes show drastic changes in gene expression in the *Sox9* cKO AVC. Surprisingly, <6% of genes with associated SOX9 peaks showed altered mRNA expression. Approximately 60% of the SOX9 target genes were downregulated. Although *in vitro* promoter analysis supported both a positive and negative role of SOX9 in gene regulation, the induction or repression of gene expression by SOX9 was at most threefold. Together, these data suggest that SOX9 might function as a modulator of gene expression rather than being required to produce large changes in gene expression. SOX9 has recently been suggested to act as a pioneer factor and has been linked with super enhancers (Adam et al., 2015), implying that SOX9 plays a role in chromatin dynamics. A recent model for SOX9 function in chondrocytes proposes two types of SOX9 interactions: Class I SOX9

Development (2015) 142, 4340-4350 doi:10.1242/dev.125252

engagement regions are TSS biased and indirectly bind SOX9 via the transcriptional machinery; Class II regions are more distally located, are directly bound by SOX9 and are enriched for skeletal enhancers (Ohba et al., 2015). Of note, most of the SOX9 peaks associated with genes that have altered gene expression in the AVC are located outside of the promoter (data not shown).

Several of these SOX9 target genes are known to be important for valve formation, including ECM-related genes and TFs. Downregulated TFs with associated SOX9 peaks included *Lef1*, *Pitx2* and *Hand2*. Loss of *Lef1* (via TBX20 deletion), *Pitx2* or *Hand2* is associated with valve defects (Liu et al., 2002; Holler et al., 2010; Cai et al., 2013). TFs with the most reduced expression in *Sox9* cKO valves were *Twist1*, *Sox4* and *Mecom*. Similar to SOX9, these three TFs are highly expressed in the cardiac cushions and mutations in each of these factors cause major valve defects, resulting in embryonic fatality (Ya et al., 1998; Vincentz et al., 2008; Bard-Chapeau et al., 2014).

SOX proteins are known to regulate TFs that will function as their future co-factors (Kamachi and Kondoh, 2013). SOX9 is known to regulate and cooperate with SOX5/6 to regulate target genes in the developing limb (Han and Lefebvre, 2008; Liu and Lefebvre, 2015) and both have associated SOX9 peaks in our limb ChIP-Seq data. Similarly, SOX9 might activate SOX4 in the heart to help co-regulate valve-specific genes. Motif analysis revealed EVI1 (protein product derived from *Mecom*) as another potential co-factor for SOX9 and comparison of EVI1 peaks in cancer cells (Bard-Chapeau et al., 2012) with SOX9 AVC peaks identified hundreds of overlapping target genes (P.A.H., V.C.G. and R.C., unpublished).

We have shown that SOX9 can modulate the levels of *Twist1* expression in the developing AVC. In the absence of SOX9, *Twist1* mRNA expression was reduced by approximately threefold in the valve mesenchyme. TWIST1 can induce proliferation and migration of valve mesenchyme during early valve formation (Shelton and Yutzey, 2008; Chakraborty et al., 2010b) and, following EMT, TWIST1 plays a role in regulating differentiation of the AVC mesenchyme (Vrljicak et al., 2012). When TWIST1 persists at later stages of valve development, it leads to increased mesenchyme proliferation, increased TBX20 expression, and primitive ECM (Chakraborty et al., 2010b). TWIST1 directly regulates *Tbx20* (Lee and Yutzey, 2011), but, of note, *Twist1*-null hearts do not show a difference in *Tbx20* levels in the AVC compared with WT (Vincentz et al., 2008). Interestingly, we found that TBX20 was downregulated in the *Sox9* cKO AVC and that SOX9 occupied regulatory regions associated with TBX20. These data suggest that TWIST1 and SOX9 might cooperate to regulate *Tbx20* in developing heart valves. Furthermore, SOX9 is downregulated in *Twist1*-null AVC (Vrljicak et al., 2012), suggesting the existence of a feedback loop between the two factors.

Taken together, our data reveal that SOX9 occupies regulatory regions and impacts the expression of key TFs that are vitally important for heart valve development (Fig. 5). Intriguingly, many of these TFs have been suggested to regulate each other's expression. For example, TWIST1 has been shown to regulate *Tbx20* (Lee and Yutzey, 2011) and TBX20 in turn has been shown to regulate LEF1 in the valve endocardial cells (Cai et al., 2013). EVI1 has been shown to regulate SOX4 and alters its expression (Bard-Chapeau et al., 2014), and EVI1 and SOX4 can collaborate together in myeloid leukemia (Boyd et al., 2006). This demonstrates that complex interactions occur at multiple levels in transcriptional regulation by SOX9 and suggests that the essential TFs are regulated in numerous ways to ensure proper valve formation. Our work suggests that SOX9 and its transcriptional target TFs form a gene regulatory network to drive valve morphogenesis. In humans, aberrant expression of SOX9 and its transcriptional targets have been associated with adult heart valve disease (Hulin et al., 2013). Thus, understanding the SOX9-initiated transcription networks in heart valve development could provide additional insights into adult heart valve disease.

MATERIALS AND METHODS

Mice

The Animal Care Committee at the University of British Columbia approved all animal procedures. C57BL/6J and ICR mice were used for ChIP-Seq and ChIP-qPCR validation, respectively. *Sox9*$^{fl/fl}$ (*B6.129S7-Sox9tm2Crm/J*) and *Tie2-Cre* [*B6.Cg-Tg(Tek-cre)12Flv/J*] mice (Jackson Laboratories) were bred as described (Lincoln et al., 2007) and genotyped (Table S1). See supplementary materials and methods for additional information.

ChIP-Seq and analysis

Three independent ChIPs generated from embryonic tissues (AVC ChIPs from 45, 45 and 74 embryos; limb ChIPs from 12, 11 and 16 limbs) were pooled for SOX9 ChIP-Seq. See supplementary materials and methods for details. ChIPs were performed as described (Vrljicak et al., 2012) with modifications (see supplementary materials and methods). Protein A/G beads (Pierce) with 3 µg of rabbit polyclonal anti-mouse SOX9 antibody (Millipore AB5535) or 3 µg of rabbit polyclonal IgG antibody (Santa Cruz sc-2027) were used. Unbound sonicated DNA was sequenced as input. ChIP-Seq libraries were constructed and sequenced at Canada's Michael Smith Genome Sciences Centre (Vancouver, BC). The Burrows-Wheeler Aligner (Li and Durbin, 2009) aligned reads to mm9. FindPeaks3.1 (Fejes et al., 2008) identified regions of enrichment or 'peaks'. An FDR was applied to threshold ChIP-Seq data (Robertson et al., 2008) and false positives were limited using input. A local z-score was calculated between peak height and control coverage and peaks below the threshold were filtered out (Fig. S1A,B). Peaks that passed filtering, z-score, peak height, and FDR-based peak height cut-offs were retained for analysis. Wig/BED files were analyzed using UCSC Genome browser (Kent et al., 2002), Galaxy (Blankenberg et al., 2010) and Cistrome (Liu et al., 2011). Peaks were associated with genes through a 'yes-no' process as depicted by the flowchart (Fig. S1D) to reduce the number of mis-associated peaks (see supplementary materials and methods for details of peak-to-gene associations). Data have been deposited in Gene Expression Omnibus under accession number GSE73225.

RNA isolation and RNA-Seq

Individual AVCs were dissected and put into Trizol (Thermo Fisher Scientific) and genotyped from unused embryonic tissue. *Sox9* cKO hearts were only taken for analysis if the heart was functional. cDNA was synthesized to confirm loss of *Sox9* in the AVCs by qRT-PCR. Two to three AVC RNA samples for each genotype were pooled. Duplicate RNA-Seq libraries were generated and sequenced on Illumina Mi-Seq or Next-Seq for each genotype. Reads were aligned with Tophat2 (Kim et al., 2013) to mm9. Fragments per kilobase of exon per million reads (FPKMs) were calculated using Cufflinks (Trapnell et al., 2010) and gene FPKMs were an average of duplicate libraries for each genotype. EdgeR (Robinson et al., 2010) was used for normalization and differential expression was determined by log2 fold change between WT and *Sox9* cKO gene values. For downstream analyses, genes had to be ≥0.5 FPKM and ≥±0.58 log2 fold change. GO analysis was performed using GOrilla (Eden et al., 2009) and Ingenuity Pathway Analysis (Qiagen). For further details, see supplementary materials and methods.

PCR, quantitative (q)RT-PCR, and ChIP-qPCR

cDNA was synthesized with Transcriptor First Strand cDNA Synthesis Kit (Roche). HiFi Taq polymerase (Thermo Fisher Scientific) was used for genotyping. Genomic DNA was isolated from embryonic tissue using

Development (2015) 142, 4340-4350 doi:10.1242/dev.125252

KAPA express extract. ChIP-qPCR and qRT-PCR were performed with FastStart Universal SYBR Master (Roche) on the ABI 7900HT Fast Real-Time PCR System. See Table S1 for primers. Taqman assays (Thermo Fisher Scientific) used Perfecta qPCR Fastmix (Quanta Biosciences). *Actb* and *Gapdh* were used for relative quantification for qRT-PCR and Taqman assays, respectively. ChIP-qPCR fold enrichment was calculated by 2ΔCt difference between IgG ChIP and SOX9 ChIP).

Immunofluorescence and *in situ* hybridization

Hearts were fixed in 4% paraformaldehyde (Sigma) overnight, subjected to a sucrose gradient, embedded in OCT (Sakura) and cryosectioned at 8 µm thickness. IF was performed as described (Chang et al., 2011). The primary antibody was rabbit anti-mouse SOX9 (Millipore AB5535; 1:600) and the secondary antibody was anti-rabbit Alexa Fluor 488 or 594 (Thermo Fisher Scientific). Rabbit anti-phospho histone H3 (Abcam) was used for proliferation assays. 4′,6-Diamidino-2-phenylindole, dihydrochloride (Sigma) was used to stain nuclei. Images were captured on a Zeiss Axioplan 2 microscope or TCS SP5 Leica confocal microscope. *In situ* hybridization was performed as described (Hou et al., 2007). Images were captured on a Zeiss Axioplan 2 microscope.

Cell culture, transfection, cloning and luciferase assays

HEK293T cells were maintained in DMEM (Stemcell) with 10% foetal bovine serum (Thermo Fisher Scientific) and transfected at 60% confluency using polyethylenimine (Polysciences) (Baker et al., 1997). Luciferase assays were performed 2 days post-transfection using the Dual-Luciferase Reporter System (Promega). Regions containing SOX9 peaks were PCR amplified (Table S1) and cloned into either a modified pGL3 promoter luciferase plasmid (Promega), containing an E1b promoter (pGL3-E1Bp; Benchabane and Wrana, 2003), for enhancers) or pGL4-basic (Promega) promoter-less vector (for promoters). Luciferase activity was tested in the presence of a pcDNA3-SOX9 expression vector (Lefebvre et al., 1997) (0.1 µg/well, 24-well plate) or pcDNA3 backbone (0.1 µg/well). Firefly luciferase activity was normalized to *Renilla* luciferase activity for each sample. Enhancer and promoter firefly luciferase activity is shown to the empty vector. *Mecom* enhancer mutants were generated using gBlocks by Integrated DNA Technologies (IDT) (Fig. S7).

Acknowledgements

We would like to thank Dr Aly Karsan for all of his excellent ideas and suggestions throughout this project. We would also like to thank Dr Amanda Kotzer for all of her help in managing this project.

Competing interests

The authors declare no competing or financial interests.

Author contributions

V.C.G., R.C., O.A. and P.A.H. contributed to the formulation and design of the experiments. V.C.G., R.C., O.A. and D.Y.L. performed the experiments. V.C.G., R.C., M.B. and R.V.W. analyzed the data. V.C.G., R.C., T.M.U. and P.A.H. contributed to the writing of the manuscript. Y.Z., S.J.M.J. and M.A.M. were involved in obtaining funding for the genome project and/or in the generation and processing of sequencing libraries.

Funding

This work was supported by a Grant-in-Aid from the Heart and Stroke Foundation of Canada [G-14-0006139]; Genome Canada; and Genome British Columbia.

Supplementary information

Supplementary information available online at
http://dev.biologists.org/lookup/suppl/doi:10.1242/dev.125252/-/DC1

References

Adam, R. C., Yang, H., Rockowitz, S., Larsen, S. B., Nikolova, M., Oristian, D. S., Polak, L., Kadaja, M., Asare, A., Zheng, D. et al. (2015). Pioneer factors govern super-enhancer dynamics in stem cell plasticity and lineage choice. *Nature* **521**, 366-370.

Akiyama, H., Chaboissier, M.-C., Martin, J. F., Schedl, A. and de Crombrugghe, B. (2002). The transcription factor Sox9 has essential roles in successive steps of the chondrocyte differentiation pathway and is required for expression of Sox5 and Sox6. *Genes Dev.* **16**, 2813-2828.

Akiyama, H., Chaboissier, M.-C., Behringer, R. R., Rowitch, D. H., Schedl, A., Epstein, J. A. and de Crombrugghe, B. (2004). Essential role of Sox9 in the pathway that controls formation of cardiac valves and septa. *Proc. Natl. Acad. Sci. USA* **101**, 6502-6507.

An, C.-I., Dong, Y. and Hagiwara, N. (2011). Genome-wide mapping of Sox6 binding sites in skeletal muscle reveals both direct and indirect regulation of muscle terminal differentiation by Sox6. *BMC Dev. Biol.* **11**, 59.

Baker, A., Saltik, M., Lehrmann, H., Killisch, I., Mautner, V., Lamm, G., Christofori, G. and Cotten, M. (1997). Polyethylenimine (PEI) is a simple, inexpensive and effective reagent for condensing and linking plasmid DNA to adenovirus for gene delivery. *Gene Ther.* **4**, 773-782.

Bard-Chapeau, E. A., Jeyakani, J., Kok, C. H., Muller, J., Chua, B. Q., Gunaratne, J., Batagov, A., Jenjaroenpun, P., Kuznetsov, V. A., Wei, C.-L. et al. (2012). Ecotopic viral integration site 1 (EVI1) regulates multiple cellular processes important for cancer and is a synergistic partner for FOS protein in invasive tumors. *Proc. Natl. Acad. Sci. USA* **109**, 2168-2173.

Bard-Chapeau, E. A., Szumska, D., Jacob, B., Chua, B. Q. L., Chatterjee, G. C., Zhang, Y., Ward, J. M., Urun, F., Kinameri, E., Vincent, S. D. et al. (2014). Mice carrying a hypomorphic Evi1 allele are embryonic viable but exhibit severe congenital heart defects. *PLoS ONE* **9**, e89397.

Bashur, L. A., Chen, D., Chen, Z., Liang, B., Pardi, R., Murakami, S. and Zhou, G. (2014). Loss of jab1 in osteochondral progenitor cells severely impairs embryonic limb development in mice. *J. Cell. Physiol.* **229**, 1607-1617.

Bell, D. M., Leung, K. K., Wheatley, S. C., Ng, L. J., Zhou, S., Wing Ling, K., Har Sham, M., Koopman, P., Tam, P. P. L. and Cheah, K. S. E. (1997). SOX9 directly regulates the type-II collagen gene. *Nat. Genet.* **16**, 174-178.

Benchabane, H. and Wrana, J. L. (2003). GATA- and Smad1-dependent enhancers in the Smad7 gene differentially interpret bone morphogenetic protein concentrations. *Mol. Cell. Biol.* **23**, 6646-6661.

Bernard, P., Tang, P., Liu, S., Dewing, P., Harley, V. R. and Vilain, E. (2003). Dimerization of SOX9 is required for chondrogenesis, but not for sex determination. *Hum. Mol. Genet.* **12**, 1755-1765.

Blankenberg, D., Von Kuster, G., Coraor, N., Ananda, G., Lazarus, R., Mangan, M., Nekrutenko, A. and Taylor, J. (2010). Galaxy: a web-based genome analysis tool for experimentalists. *Curr. Protoc. Mol. Biol.* **89**, 19.10.1-19.10.21.

Boyd, K. E., Xiao, Y.-Y., Fan, K., Poholek, A., Copeland, N. G., Jenkins, N. A. and Perkins, A. S. (2006). Sox4 cooperates with Evi1 in AKXD-23 myeloid tumors via transactivation of proviral LTR. *Blood* **107**, 733-741.

Bracken, A. P., Pasini, D., Capra, M., Prosperini, E., Colli, E. and Helin, K. (2003). EZH2 is downstream of the pRB-E2F pathway, essential for proliferation and amplified in cancer. *EMBO J.* **22**, 5323-5335.

Bridgewater, L. C., Lefebvre, V. and de Crombrugghe, B. (1998). Chondrocyte-specific enhancer elements in the Col11a2 gene resemble the Col2a1 tissue-specific enhancer. *J. Biol. Chem.* **273**, 14998-15006.

Cai, X., Zhang, W., Hu, J., Zhang, L., Sultana, N., Wu, B., Cai, W., Zhou, B. and Cai, C.-L. (2013). Tbx20 acts upstream of Wnt signaling to regulate endocardial cushion formation and valve remodeling during mouse cardiogenesis. *Development* **140**, 3176-3187.

Chakraborty, S., Combs, M. D. and Yutzey, K. E. (2010a). Transcriptional regulation of heart valve progenitor cells. *Pediatr. Cardiol.* **31**, 414-421.

Chakraborty, S., Wirrig, E. E., Hinton, R. B., Merrill, W. H., Spicer, D. B. and Yutzey, K. E. (2010b). Twist1 promotes heart valve cell proliferation and extracellular matrix gene expression during development in vivo and is expressed in human diseased aortic valves. *Dev. Biol.* **347**, 167-179.

Chang, A. C. Y., Fu, Y., Garside, V. C., Niessen, K., Chang, L., Fuller, M., Setiadi, A., Smrz, J., Kyle, A., Minchinton, A. et al. (2011). Notch initiates the endothelial-to-mesenchymal transition in the atrioventricular canal through autocrine activation of soluble guanylyl cyclase. *Dev. Cell* **21**, 288-300.

Chang, A. C. Y., Garside, V. C., Fournier, M., Smrz, J., Vrljicak, P., Umlandt, P., Fuller, M., Robertson, G., Zhao, Y., Tam, A. et al. (2014). A Notch-dependent transcriptional hierarchy promotes mesenchymal transdifferentiation in the cardiac cushion. *Dev. Dyn.* **243**, 894-905.

Claret, F.-X., Hibi, M., Dhut, S., Toda, T. and Karin, M. (1996). A new group of conserved coactivators that increase the specificity of AP-1 transcription factors. *Nature* **383**, 453-457.

de Vlaming, A., Sauls, K., Hajdu, Z., Visconti, R. P., Mehesz, A. N., Levine, R. A., Slaugenhaupt, S. A., Hagège, A., Chester, A. H., Markwald, R. R. et al. (2012). Atrioventricular valve development: new perspectives on an old theme. *Differentiation* **84**, 103-116.

Eden, E., Navon, R., Steinfeld, I., Lipson, D. and Yakhini, Z. (2009). GOrilla: a tool for discovery and visualization of enriched GO terms in ranked gene lists. *BMC Bioinformatics* **10**, 48.

Fejes, A. P., Robertson, G., Bilenky, M., Varhol, R., Bainbridge, M. and Jones, S. J. (2008). FindPeaks 3.1: a tool for identifying areas of enrichment from massively parallel short-read sequencing technology. *Bioinformatics* **24**, 1729-1730.

Giono, L. E. and Manfredi, J. J. (2006). The p53 tumor suppressor participates in multiple cell cycle checkpoints. *J. Cell Physiol.* **209**, 13-20.

Development (2015) 142, 4340-4350 doi:10.1242/dev.125252

Han, Y. and Lefebvre, V. (2008). L-Sox5 and Sox6 drive expression of the aggrecan gene in cartilage by securing binding of Sox9 to a far-upstream enhancer. *Mol. Cell. Biol.* **28**, 4999-5013.
Holler, K. L., Hendershot, T. J., Troy, S. E., Vincentz, J. W., Firulli, A. B. and Howard, M. J. (2010). Targeted deletion of Hand2 in cardiac neural crest-derived cells influences cardiac gene expression and outflow tract development. *Dev. Biol.* **341**, 291-304.
Hou, J., Charters, A. M., Lee, S. C., Zhao, Y., Wu, M. K., Jones, S. J. M., Marra, M. A. and Hoodless, P. A. (2007). A systematic screen for genes expressed in definitive endoderm by Serial Analysis of Gene Expression (SAGE). *BMC Dev. Biol.* **7**, 92.
Hoyt, P. R., Bartholomew, C., Davis, A. J., Yutzey, K., Gamer, L. W., Potter, S. S., Ihle, J. N. and Mucenski, M. L. (1997). The Evil proto-oncogene is required at midgestation for neural, heart, and paraxial mesenchyme development. *Mech. Dev.* **65**, 55-70.
Huang, W., Zhou, X., Lefebvre, V. and de Crombrugghe, B. (2000). Phosphorylation of SOX9 by cyclic AMP-dependent protein kinase A enhances SOX9's ability to transactivate a Col2a1 chondrocyte-specific enhancer. *Mol. Cell. Biol.* **20**, 4149-4158.
Hulin, A., Deroanne, C., Lambert, C., Defraigne, J.-O., Nusgens, B., Radermecker, M. and Colige, A. (2013). Emerging pathogenic mechanisms in human myxomatous mitral valve: lessons from past and novel data. *Cardiovasc. Pathol.* **22**, 245-250.
Jain, V. and Sen, B. (2014). Campomelic dysplasia. *J. Pediatr. Orthop. B* **23**, 485-488.
Jang, S.-W., Liu, X., Fu, H., Rees, H., Yepes, M., Levey, A. and Ye, K. (2009). Interaction of Akt-phosphorylated SRPK2 with 14-3-3 mediates cell cycle and cell death in neurons. *J. Biol. Chem.* **284**, 24512-24525.
Kadaja, M., Keyes, B. E., Lin, M., Pasolli, H. A., Genander, M., Polak, L., Stokes, N., Zheng, D. and Fuchs, E. (2014). SOX9: a stem cell transcriptional regulator of secreted niche signaling factors. *Genes Dev.* **28**, 328-341.
Kamachi, Y. and Kondoh, H. (2013). Sox proteins: regulators of cell fate specification and differentiation. *Development* **140**, 4129-4144.
Kang, P., Lee, H. K., Glasgow, S. M., Finley, M., Donti, T., Gaber, Z. B., Graham, B. H., Foster, A. E., Novitch, B. G., Gronostajski, R. M. et al. (2012). Sox9 and NFIA coordinate a transcriptional regulatory cascade during the initiation of gliogenesis. *Neuron* **74**, 79-94.
Kelly, R. D. W. and Cowley, S. M. (2013). The physiological roles of histone deacetylase (HDAC) 1 and 2: complex co-stars with multiple leading parts. *Biochem. Soc. Trans.* **41**, 741-749.
Kent, W. J., Sugnet, C. W., Furey, T. S., Roskin, K. M., Pringle, T. H., Zahler, A. M. and Haussler, D. (2002). The human genome browser at UCSC. *Genome Res.* **12**, 996-1006.
Kim, D., Pertea, G., Trapnell, C., Pimentel, H., Kelley, R. and Salzberg, S. L. (2013). TopHat2: accurate alignment of transcriptomes in the presence of insertions, deletions and gene fusions. *Genome Biol.* **14**, R36.
Kisanuki, Y. Y., Hammer, R. E., Miyazaki, J.-i., Williams, S. C., Richardson, J. A. and Yanagisawa, M. (2001). Tie2-Cre transgenic mice: a new model for endothelial cell-lineage analysis in vivo. *Dev. Biol.* **230**, 230-242.
Lee, M. P. and Yutzey, K. E. (2011). Twist1 directly regulates genes that promote cell proliferation and migration in developing heart valves. *PLoS ONE* **6**, e29758.
Lefebvre, V., Huang, W., Harley, V. R., Goodfellow, P. N. and de Crombrugghe, B. (1997). SOX9 is a potent activator of the chondrocyte-specific enhancer of the pro alpha1(II) collagen gene. *Mol. Cell. Biol.* **17**, 2336-2346.
Li, H. and Durbin, R. (2009). Fast and accurate short read alignment with Burrows-Wheeler transform. *Bioinformatics* **25**, 1754-1760.
Lincoln, J., Lange, A. W. and Yutzey, K. E. (2006). Hearts and bones: shared regulatory mechanisms in heart valve, cartilage, tendon, and bone development. *Dev. Biol.* **294**, 292-302.
Lincoln, J., Kist, R., Scherer, G. and Yutzey, K. E. (2007). Sox9 is required for precursor cell expansion and extracellular matrix organization during mouse heart valve development. *Dev. Biol.* **305**, 120-132.
Liu, C.-F. and Lefebvre, V. (2015). The transcription factors SOX9 and SOX5/SOX6 cooperate genome-wide through super-enhancers to drive chondrogenesis. *Nucleic Acids Res.* **43**, 8183-8203.
Liu, C., Liu, W., Palie, J., Lu, M. F., Brown, N. A. and Martin, J. F. (2002). Pitx2c patterns anterior myocardium and aortic arch vessels and is required for local cell movement into atrioventricular cushions. *Development* **129**, 5081-5091.
Liu, T., Ortiz, J. A., Taing, L., Meyer, C. A., Lee, B., Zhang, Y., Shin, H., Wong, S. S., Ma, J., Lei, Y. et al. (2011). Cistrome: an integrative platform for transcriptional regulation studies. *Genome Biol.* **12**, R83.
McAninch, D. and Thomas, P. (2014). Identification of highly conserved putative developmental enhancers bound by SOX3 in neural progenitors using ChIP-Seq. *PLoS ONE* **9**, e113361.
Montero, J. A., Giron, B., Arrechedera, H., Cheng, Y.-C., Scotting, P., Chimal-Monroy, J., Garcia-Porrero, J. A. and Hurle, J. M. (2002). Expression of Sox8, Sox9 and Sox10 in the developing valves and autonomic nerves of the embryonic heart. *Mech. Dev.* **118**, 199-202.
Nagy, A., Kenesi, E., Rentsendorj, O., Molnar, A., Szenasi, T., Sinko, I., Zvara, A., Oommen, S. T., Barta, E., Puskas, L. G. et al. (2011). Evolutionarily conserved, growth plate zone-specific regulation of the matrilin-1 promoter: L-Sox5/Sox6 and Nfi factors bound near TATA finely tune activation by Sox9. *Mol. Cell. Biol.* **31**, 686-699.
Ohba, S., He, X., Hojo, H. and McMahon, A. P. (2015). Distinct transcriptional programs underlie Sox9 regulation of the mammalian chondrocyte. *Cell Rep.* **12**, 229-243.
Person, A. D., Klewer, S. E. and Runyan, R. B. (2005). Cell biology of cardiac cushion development. *Int. Rev. Cytol.* **243**, 287-335.
Pritchett, J., Athwal, V., Roberts, N., Hanley, N. A. and Hanley, K. P. (2011). Understanding the role of SOX9 in acquired diseases: lessons from development. *Trends Mol. Med.* **17**, 166-174.
Robertson, A. G., Bilenky, M., Tam, A., Zhao, Y., Zeng, T., Thiessen, N., Cezard, T., Fejes, A. P., Wederell, E. D., Cullum, R. et al. (2008). Genome-wide relationship between histone H3 lysine 4 mono- and tri-methylation and transcription factor binding. *Genome Res.* **18**, 1906-1917.
Robinson, M. D., McCarthy, D. J. and Smyth, G. K. (2010). edgeR: a Bioconductor package for differential expression analysis of digital gene expression data. *Bioinformatics* **26**, 139-140.
Rockich, B. E., Hrycaj, S. M., Shih, H. P., Nagy, M. S., Ferguson, M. A. H., Kopp, J. L., Sander, M., Wellik, D. M. and Spence, J. R. (2013). Sox9 plays multiple roles in the lung epithelium during branching morphogenesis. *Proc. Natl. Acad. Sci. USA* **110**, E4456-E4464.
Sekiya, I., Tsuji, K., Koopman, P., Watanabe, H., Yamada, Y., Shinomiya, K., Nifuji, A. and Noda, M. (2000). SOX9 enhances aggrecan gene promoter/enhancer activity and is up-regulated by retinoic acid in a cartilage-derived cell line, TC6. *J. Biol. Chem.* **275**, 10738-10744.
Shaulian, E. (2010). AP-1 — The Jun proteins: oncogenes or tumor suppressors in disguise? *Cell. Signal.* **22**, 894-899.
Shelton, E. L. and Yutzey, K. E. (2008). Twist1 function in endocardial cushion cell proliferation, migration, and differentiation during heart valve development. *Dev. Biol.* **317**, 282-295.
Shi, Z., Chiang, C.-I., Labhart, P., Zhao, Y., Yang, J., Mistretta, T.-A., Henning, S. J., Maity, S. N. and Mori-Akiyama, Y. (2015). Context-specific role of SOX9 in NF-Y mediated gene regulation in colorectal cancer cells. *Nucleic Acids Res.* **43**, 6257-6269.
Snarr, B. S., Kern, C. B. and Wessels, A. (2008). Origin and fate of cardiac mesenchyme. *Dev. Dyn.* **237**, 2804-2819.
Stockl, S., Bauer, R. J., Bosserhoff, A. K., Gottl, C., Grifka, J. and Grassel, S. (2013). Sox9 modulates cell survival and adipogenic differentiation of multipotent adult rat mesenchymal stem cells. *J. Cell Sci.* **126**, 2890-2902.
Stork, P. J. S. and Schmitt, J. M. (2002). Crosstalk between cAMP and MAP kinase signaling in the regulation of cell proliferation. *Trends Cell Biol.* **12**, 258-266.
Timmerman, L. A., Grego-Bessa, J., Raya, A., Bertrán, E., Pérez-Pomares, J. M., Díez, J., Aranda, S., Palomo, S., McCormick, F., Izpisúa-Belmonte, J. C. et al. (2004). Notch promotes epithelial-mesenchymal transition during cardiac development and oncogenic transformation. *Genes Dev.* **18**, 99-115.
Trapnell, C., Williams, B. A., Pertea, G., Mortazavi, A., Kwan, G., van Baren, M. J., Salzberg, S. L., Wold, B. J. and Pachter, L. (2010). Transcript assembly and quantification by RNA-Seq reveals unannotated transcripts and isoform switching during cell differentiation. *Nat. Biotechnol.* **28**, 511-515.
Trowe, M.-O., Shah, S., Petry, M., Airik, R., Schuster-Gossler, K., Kist, R. and Kispert, A. (2010). Loss of Sox9 in the periotic mesenchyme affects mesenchymal expansion and differentiation, and epithelial morphogenesis during cochlea development in the mouse. *Dev. Biol.* **342**, 51-62.
Vincentz, J. W., Barnes, R. M., Rodgers, R., Firulli, B. A., Conway, S. J. and Firulli, A. B. (2008). An absence of Twist1 results in aberrant cardiac neural crest morphogenesis. *Dev. Biol.* **320**, 131-139.
Vrljicak, P., Cullum, R., Xu, E., Chang, A. C. Y., Wederell, E. D., Bilenky, M., Jones, S. J. M., Marra, M. A., Karsan, A. and Hoodless, P. A. (2012). Twist1 transcriptional targets in the developing atrio-ventricular canal of the mouse. *PLoS ONE* **7**, e40815.
Wagner, T., Wirth, J., Meyer, J., Zabel, B., Held, M., Zimmer, J., Pasantes, J., Bricarelli, F. D., Keutel, J., Hustert, E. et al. (1994). Autosomal sex reversal and campomelic dysplasia are caused by mutations in and around the SRY-related gene SOX9. *Cell* **79**, 1111-1120.
Wheatley, S., Wright, E., Jeske, Y., Mccormack, A., Bowles, J. and Koopman, P. (1996). Aetiology of the skeletal dysmorphology syndrome campomelic dysplasia: expression of the Sox9 gene during chondrogenesis in mouse embryos. *Ann. N. Y. Acad. Sci.* **785**, 350-352.
Xu, N., Lao, Y., Zhang, Y. and Gillespie, D. A. (2012). Akt: a double-edged sword in cell proliferation and genome stability. *J. Oncol.* **2012**, 951724.
Ya, J., Schilham, M. W., de Boer, P. A., Moorman, A. F. M., Clevers, H. and Lamers, W. H. (1998). Sox4-deficiency syndrome in mice is an animal model for common trunk. *Circ. Res.* **83**, 986-994.

SUPPLEMENTAL MATERIAL

Methods:

Mice strains and tissue dissection

All animal protocols were approved by the Animal Care Committee at the University of British Columbia. C57BL/6J mice were used for all ChIP-Seq libraries. ICR mice were used for ChIP-qPCR validation. To generate *Sox9fl/fl* (WT) and *Sox9fl/f;Tek-Cre/+* (*Sox9* cKO) embryos, *Sox9fl/fl* female mice were crossed with *Tie2-Cre* male mice to generate *Sox9fl/+;Tie2-Cre* male and then *Sox9fl/+;Tie2-Cre* male mice were mated back to *Sox9fl/fl* female mice. All mice were backcrossed more than seven generations. *Sox9fl/fl* (*B6.129S7-Sox9tm2Crm/J*) and *Tie2-Cre (B6.Cg-Tg(Tek-cre) 12Flv/J)* mice were obtained from Jackson Laboratories (Sacramento, USA). The *Sox9fl* allele was genotyped using primers specific to the flox region and *Tie2-Cre* was detected using primers specific to *Cre recombinase* (Table S1). Embryos from timed matings were considered embryonic day (E) 0.5 at noon of the day a vaginal plug was observed. For the SOX9 ChIP-Seq libraries, the atrioventricular canal (AVC) and limb buds were manually dissected using forceps and a dissecting microscope. Whole hearts and heart regions including the AVC, atria, ventricles, and outflow tract were manually dissected from *Sox9fl/fl* and *Sox9fl/fl;Tek-Cre/+* embryos for immunofluorescence, qRT-PCR, and RNA-Seq libraries. *Sox9fl/fl* and *Sox9fl/+;Tie2-Cre* mice were maintained on a C57BL6 background.

Chromatin Immunoprecipitation coupled with high-throughput sequencing (ChIP-Seq)

Three independent ChIPs generated from pooled embryos were combined for SOX9 ChIP-Seq libraries. For the AVC ChIP-Seq libraries, ChIP#1 used 45 AVCs (4.64 µg chromatin), ChIP #2 used 45 AVCs (4.64 µg chromatin) and ChIP#3 used 74 AVCs (7.69 µg chromatin). Limb ChIPs pooled for the ChIP-Seq library came from 12 limbs (65.7 µg), 11 limbs (48.7 µg) and 16 limbs (68.0 µg). For all ChIP experiments, tissues were homogenized in 1% formaldehyde and incubated at room temperature (RT) for 10 min. Samples were incubated with 0.125 M glycine at RT for 5 min. Following pelleting and washing, samples were resuspended in 5 cell pellet volumes of ChIP cell lysis buffer (10 mM Tris-HCl, pH 8.0, 10 mM NaCl, 3 mM $MgCl_2$, 0.5% NP-40) with a protease inhibitor cocktail (PIC, Roche). Cells were re-homogenized and put on ice for 15 min. Cells were pelleted again and resuspended in 3 volumes of ChIP nuclear lysis buffer (1% SDS, 5 mM EDTA, 50 mM Tris-HCl, pH 8.1) containing a protease inhibitor cocktail (Roche). Following a 30-60 min incubation on ice, samples were sonicated (Sonicator 3000, Misonix) in an ice water bath for 20 cycles of 30 s on, 40 s off. After a 10 min centrifugation (4˚C, 13.2krpm) to remove cellular debris, sonicated chromatin was precleared with 20 µl Protein A/G beads (ThermoFisher Scientific, 53135), 10 µl 10x PIC and ChIP dilution buffer (with a volume equal to 4x that of the chromatin volume used, 0.01% SDS, 1.1% Triton X-100, 167 mM NaCl, 16.7 mM Tris–HCl, pH 8.1) for 1 hr, 4˚C with rotation. After 2 min 4000 rpm centrifugation, diluted chromatin removed from beads and transferred to new tubes and antibodies were added as follows: 3 µg of rabbit polyclonal anti-mouse SOX9 antibody (Millipore AB5535) or for negative controls 3 µg of normal rabbit IgG antibody (Santa Cruz, sc-2027). Samples were incubated overnight while rotating at 4˚C. Simultaneously, 20 µl of fresh Protein A/G beads (ThermoFisher Scientific) were blocked with 1 mg/ml BSA and 0.1 mg/ml herring sperm DNA in ChIP dilution buffer overnight at 4˚C. The following day, samples were incubated with blocked Protein A/G beads for four hours rotating at 4˚C. Beads were washed with several buffers as follows: low salt buffer (0.1% SDS, 1% Triton X-100, 2 mM EDTA, 20 mM Tris-HCl, pH 8.1, 150 mM NaCl), high salt buffer (low salt buffer with 500 mM NaCl), lithium chloride buffer (0.25 M LiCl, 1% NP-40, 1% deoxycholate, 1 mM EDTA, 10 mM Tris-HCl, pH 8.1) and two final washes with TE buffer. 125 µl elution buffer (1% SDS, 0.1 M NaHCO3) was added to

remove the bound chromatin-antibody complexes from the beads and samples were rotated at RT for 15 min and after centrifugation the eluted solution was removed from the beads. This was repeated. To reverse the crosslinking and break the complex bonds, 10 µl 5M NaCl, 10 µl 1M Tris-HCl (pH 6.5), 5 µl 0.5M EDTA, 1 µl Proteinase K (20mg/ml), and 2.5 µl RNAseA (10mg/ml) was added to each of the samples and incubated at 65˚C overnight. Purification of DNA was performed with two rounds of phenol-chloroform extraction and ethanol precipitation. Samples were spun down and pellets were resuspended in 50 µl dH2O. A sample of unbound sonicated DNA served as input for sequencing. ChIPs intended for ChIP-Seq libraries were validated by qPCR prior to library construction and sequencing.

ChIP DNA was sent to the Genome Sciences Centre (Vancouver, BC) for library generation. DNA was purified using 8-12% PAGE to isolate 100-300bp fragments for short read (50bp) sequencing on an Illumina Genome Analyzer (GA2) as described previously (Robertson et al., 2007). The Burrows-Wheeler Aligner (Li and Durbin, 2009) aligned reads to the mouse genome (mm9) and unmapped and/or duplicate reads were removed. FindPeaks3.1 (Fejes et al., 2008) created virtual fragments by directionally extending uniquely mapped reads to a constant length (200bp). Virtual fragments were profiled across the genome to identify regions of enrichment or “peaks”. A False Discovery Rate (FDR) was applied to threshold ChIP-Seq data as described (Robertson et al., 2008) and false positives were limited using sequenced control data (input DNA). For each ChIP-Seq peak that passed the FDR ~0.01 threshold, we found the maximal coverage of the control sample in the region +/-300bp. A local z-score was calculated between the peak height and control coverage and peaks below the threshold were filtered out. All peaks overlapping a control peak that had a height of 30 or more were also eliminated. Peaks that passed all filtering, z-score, peak height, FDR based peak height cut-offs were retained for analysis (Fig.S1A,B). Peak edges were refined by using a percentage of the maximum peak height to determine the peak edge cut off point. For each dataset, different criteria were used due to differences in sequencing depth and background noise. For screenshots and visual comparisons, we used unthresholded big wig or bed files. All sequencing data has been deposited to GEO (GSE73225).

Bioinformatic analysis of ChIP-Seq

Wig and BED files generated by FindPeaks3.1 were analyzed using tools in UCSC Genome browser (Kent et al., 2002) (http://genome.ucsc.edu/), Galaxy (Blankenberg et al., 2010) (http://main.g2.bx.psu.edu/), and Cistrome (Liu et al., 2011) (http://cistrome.dfci.harvard.edu/).

SOX9 bound regions (peaks) were associated with genes through a ‘yes-no’ process as depicted by the flowchart (Fig. S1D). Using manual methods and tools in Galaxy/Cistrome, we first identified whether the peak localized within the proximal promoter of a gene (less than 5kb upstream from a TSS or 1kb into a gene). For those that were, we checked whether the peak localized to the proximal promoter of more than one gene: those that did we associated with both genes. Peaks found to be within this region were further categorized as either at the TSS (within +/-100bp), within the first 1kb of a gene, or less than 5kb upstream from the TSS. Those that did not localize to a proximal promoter region were then scrutinized for their relationship to intragenic regions of the genome. If the peak was found within a gene region, it was categorized appropriately as 1-5kb from the TSS into the gene, midgene (more than 5kb from either end), less than 5kb from the TTS, or at the TTS (+/-100bp). Next, the remaining peaks that had not yet been categorized were associated with the closest gene in either direction. Those that were less than 10kb from a TSS were classified as being in the distal promoter. Peaks not found in the above categories were therefore found in intergenic regions. They were further categorized as either being more than 10kb from a TSS, within 5kb of a TTS and more than 5kb down from a TTS. Of note, in the rare case where the difference between the distances from the intergenic peaks to the upstream and downstream genes was less than 5kb, peaks were associated with both genes. Peaks were associated with the gene(s) that defined the genomic category of the

peak. This mapping strategy allowed us to more confidently find the best gene-to-peak association. Cistrome's SeqPos tool (Liu et al., 2011) and Screen Motif tool were used for motif analysis of SOX9 peaks. Positional Weight Matrices (PWMs) for the SOX monomer and dimer motifs were generated by SeqPos. PWMs used in Screen Motif were based on highest enrichment, p-value and top z-score.

RNA isolation and RNA-Seq

AVCs were dissected out from the heart of embryos generated from crossing *Sox9fl/fl* females and *Sox9fl/+;Tie2-Cre* male mice. Each AVC was directly placed into Trizol (ThermoFisher Scientific) and stored at -80˚C until embryos were genotyped using unused portions of each embryo. RNA was isolated with Trizol using the manufacturer's protocol. For RNA-Seq libraries, a portion of RNA from each AVC was used to synthesize cDNA (see qRT-PCR method section) for Taqman assays to confirm efficient loss of *Sox9* in the *Sox9* cKO AVCs. RNA from two or three littermate AVCs with enrichment (WT, *Sox9fl/fl*) or loss (*Sox9* cKO) of *Sox9* in the AVC were pooled together. Pooled AVC RNA samples were further purified by GeneJet clean up and concentration micro kit (ThermoFisher Scientific). RNA quality was assessed on the BioAnalyzer (Agilent Technologies) and all samples had scores over 8.7 with a required passing score of 7. Duplicate RNA-Seq libraries for each genotype were generated and sequenced using Illumina Mi-Seq or Next-Seq. Sequence reads were aligned with the Tophat2 tool (Kim et al., 2013) on Galaxy using the mouse reference genome mm9 (NCBI build 37) to generate BAM files. Aligned data from all four libraries were analyzed and Fragments per Kilobase of exon per Million reads (FPKMs) were calculated using Cufflinks (Trapnell et al., 2010). Normalized differential expression between WT and *Sox9* cKO RNA-Seq libraries was determined using edgeR (Robinson et al., 2010) in R studio (Trapnell et al., 2010). Gene FPKMs from Cufflinks were determined from the duplicate libraries for each genotype. For genes to be included for downstream analyses several criteria needed to be met: greater than or equal to 0.5 FPKM in either library, at least a 1.5 fold change (up or down) between *Sox9* cKO and WT AVC, and no zero values for expression. Cistrome and Galaxy were used to determine differential genes that were associated with SOX9 peaks.

Gene Ontology (GO) analysis was performed using GOrilla (Eden et al., 2009). Mouse genes were used as background. Lists were ranked using p-value and top categories were filtered for redundancy. Ingenuity Pathway Analysis (Qiagen) biofunctions was used for GO analysis on SOX9 target genes overlapping in all libraries and to generate an interaction network of the biofunctions: transcription, cardiogenesis, and abnormal morphology of the heart on down-regulated SOX9 targets in the heart.

References for Methods:

Blankenberg, D., Von Kuster, G., Coraor, N., Ananda, G., Lazarus, R., Mangan, M., Nekrutenko, A. and Taylor, J. (2010). Galaxy: a web-based genome analysis tool for experimentalists. *Curr Protoc Mol Biol* **Chapter 19**, Unit 19 10 11-21.

Eden, E., Navon, R., Steinfeld, I., Lipson, D. and Yakhini, Z. (2009). GOrilla: a tool for discovery and visualization of enriched GO terms in ranked gene lists. *BMC Bioinformatics* **10**, 48.

Fejes, A. P., Robertson, G., Bilenky, M., Varhol, R., Bainbridge, M. and Jones, S. J. (2008). FindPeaks 3.1: a tool for identifying areas of enrichment from massively parallel short-read sequencing technology. *Bioinformatics* **24**, 1729-1730.

Kent, W. J., Sugnet, C. W., Furey, T. S., Roskin, K. M., Pringle, T. H., Zahler, A. M. and Haussler, D. (2002). The human genome browser at UCSC. *Genome research* **12**, 996-1006.

Kim, D., Pertea, G., Trapnell, C., Pimentel, H., Kelley, R. and Salzberg, S. L. (2013). TopHat2: accurate alignment of transcriptomes in the presence of insertions, deletions and gene fusions. *Genome Biol* **14**, R36.
Li, H. and Durbin, R. (2009). Fast and accurate short read alignment with Burrows-Wheeler transform. *Bioinformatics* **25**, 1754-1760.
Liu, T., Ortiz, J. A., Taing, L., Meyer, C. A., Lee, B., Zhang, Y., Shin, H., Wong, S. S., Ma, J., Lei, Y. et al. (2011). Cistrome: an integrative platform for transcriptional regulation studies. *Genome Biol* **12**, R83.
Robertson, A. G., Bilenky, M., Tam, A., Zhao, Y., Zeng, T., Thiessen, N., Cezard, T., Fejes, A. P., Wederell, E. D., Cullum, R. et al. (2008). Genome-wide relationship between histone H3 lysine 4 mono- and tri-methylation and transcription factor binding. *Genome research* **18**, 1906-1917.
Robertson, G., Hirst, M., Bainbridge, M., Bilenky, M., Zhao, Y., Zeng, T., Euskirchen, G., Bernier, B., Varhol, R., Delaney, A. et al. (2007). Genome-wide profiles of STAT1 DNA association using chromatin immunoprecipitation and massively parallel sequencing. *Nat Methods* **4**, 651-657.
Robinson, M. D., McCarthy, D. J. and Smyth, G. K. (2010). edgeR: a Bioconductor package for differential expression analysis of digital gene expression data. *Bioinformatics (Oxford, England)* **26**, 139-140.
Trapnell, C., Williams, B. A., Pertea, G., Mortazavi, A., Kwan, G., van Baren, M. J., Salzberg, S. L., Wold, B. J. and Pachter, L. (2010). Transcript assembly and quantification by RNA-Seq reveals unannotated transcripts and isoform switching during cell differentiation. *Nat Biotechnol* **28**, 511-515.

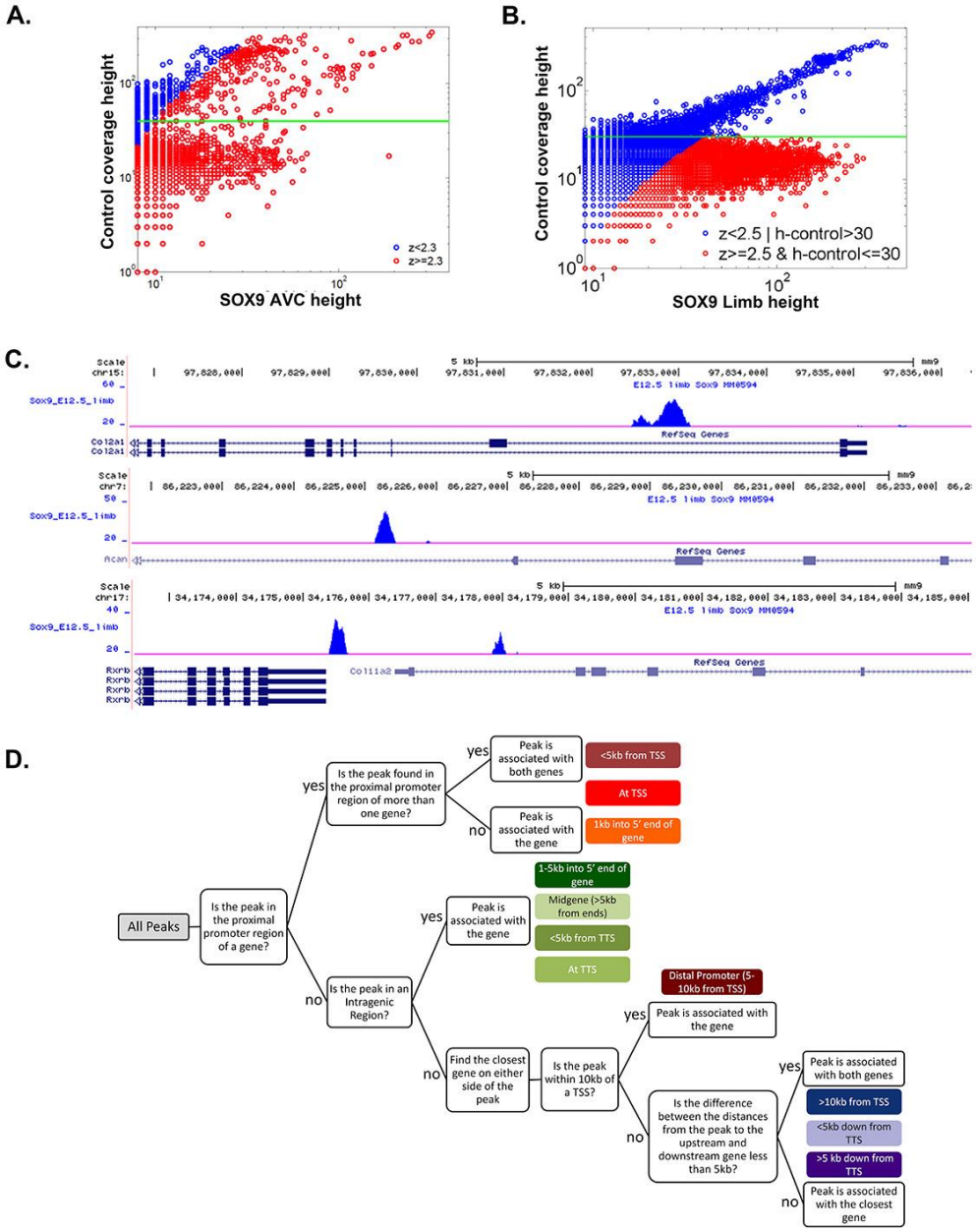

Fig.S1 Specificity of SOX9 ChIP-Seq libraries and gene associations. A. Comparison of control coverage peak height versus SOX9 E12.5 AVC or **B.** E12.5 limb peak height. Local z-score calculations determined thresholds and filtration strategies for peak inclusion in downstream analysis. **C.** UCSC genome browser screenshots of SOX9 E12.5 limb ChIP-Seq peaks for known SOX9 limb binding sites in target genes: *Col2a1*, *Acan*, *Col11a2*. **D.** A schematic showing the 'yes-no' process used to categorize SOX9 peaks to genomic regions. This process was also used to identify potential SOX9 target genes.

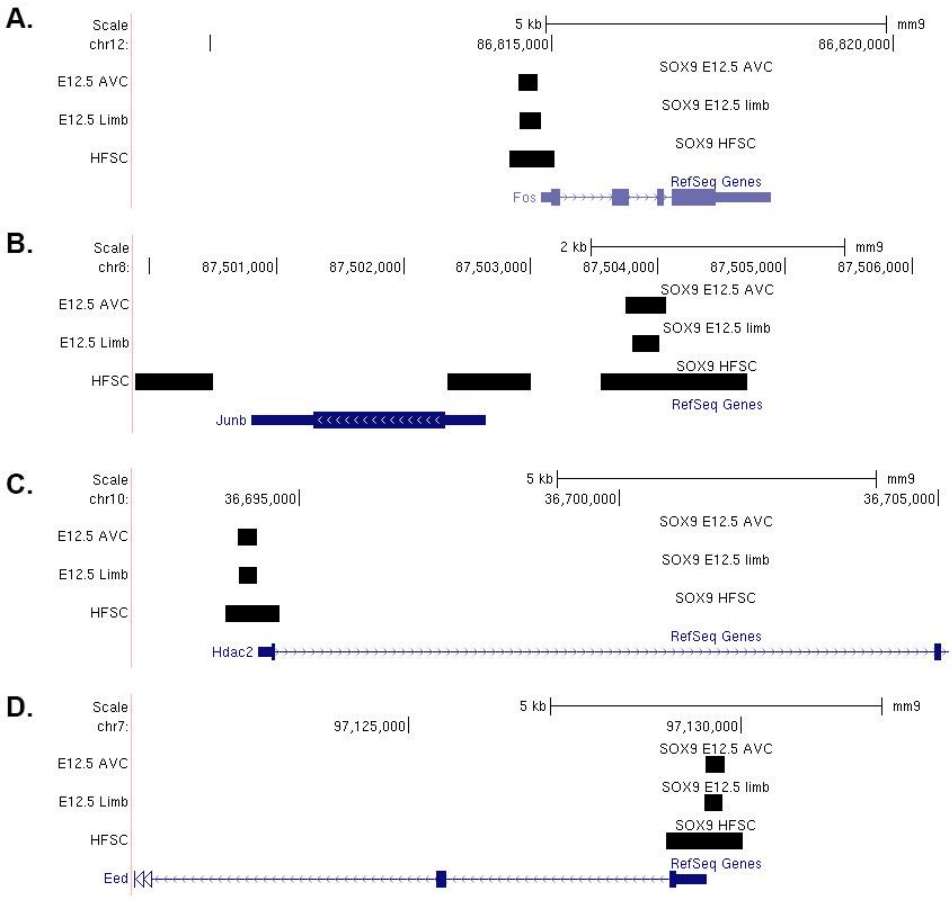

Fig.S2 Overlapping SOX9 peaks in the E12.5 AVC, E12.5 limb, and hair follicle stem cells (HF-SCs). UCSC genome browser screenshots of genes bound by SOX9 in all three ChIP-Seq libraries (E12.5 AVC, E12.5 limb, HF-SCs) using BED files (black rectangles represent peak regions) in **A.** *Fos*, **B.** *Junb*, **C.** *Hdac2*, **D.** *Eed*.

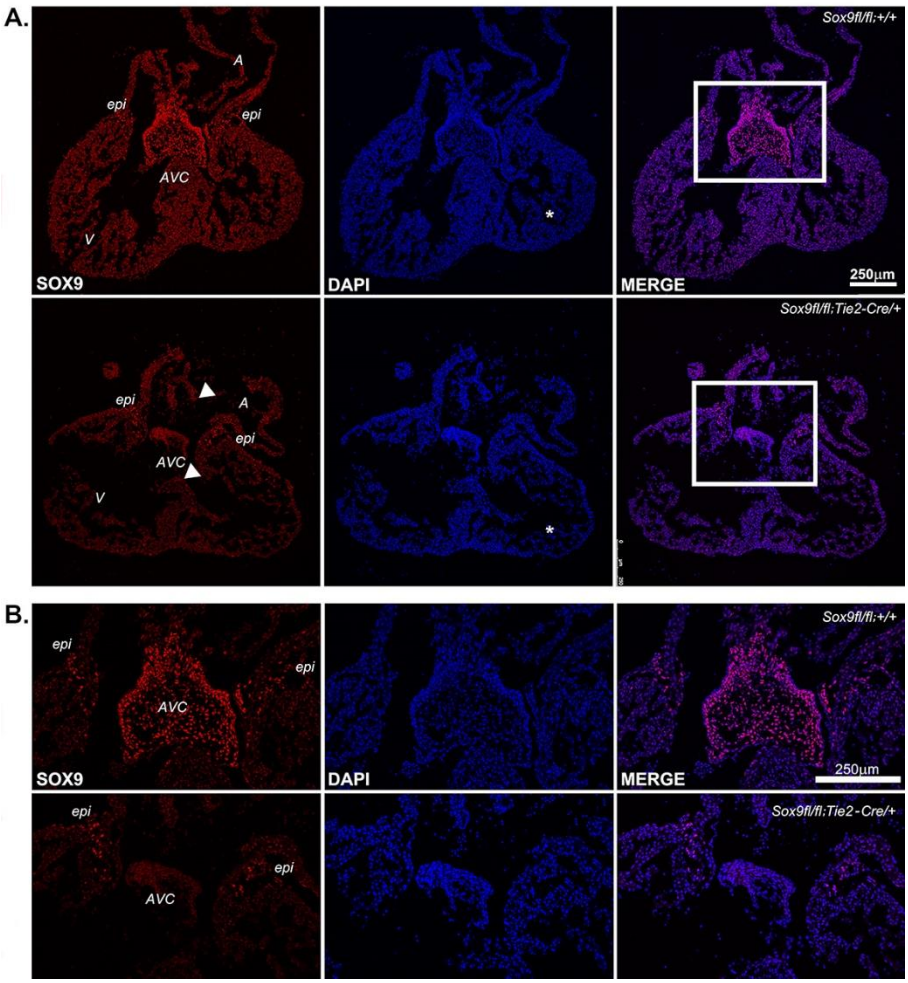

Fig.S3 Loss of SOX9 protein in developing heart valves causes major valve defects. Immunofluorescence for SOX9 on **A.** E12.5 heart and **B.** AVC (magnified from A) on *Sox9fl/fl* (WT) and *Sox9fl/fl;Tie2-Cre* (*Sox9* cKO). Arrowheads indicate the unfused septum. Asterisk indicates the myocardium. Images were taken with a Leica TCS SP5 confocal microscope. A =atria, V =ventricle, epi =epicardium. Although there is some variability due to *Cre* excision of *Sox9,* the image is a representative SOX9 expression analysis of many hearts (10+).

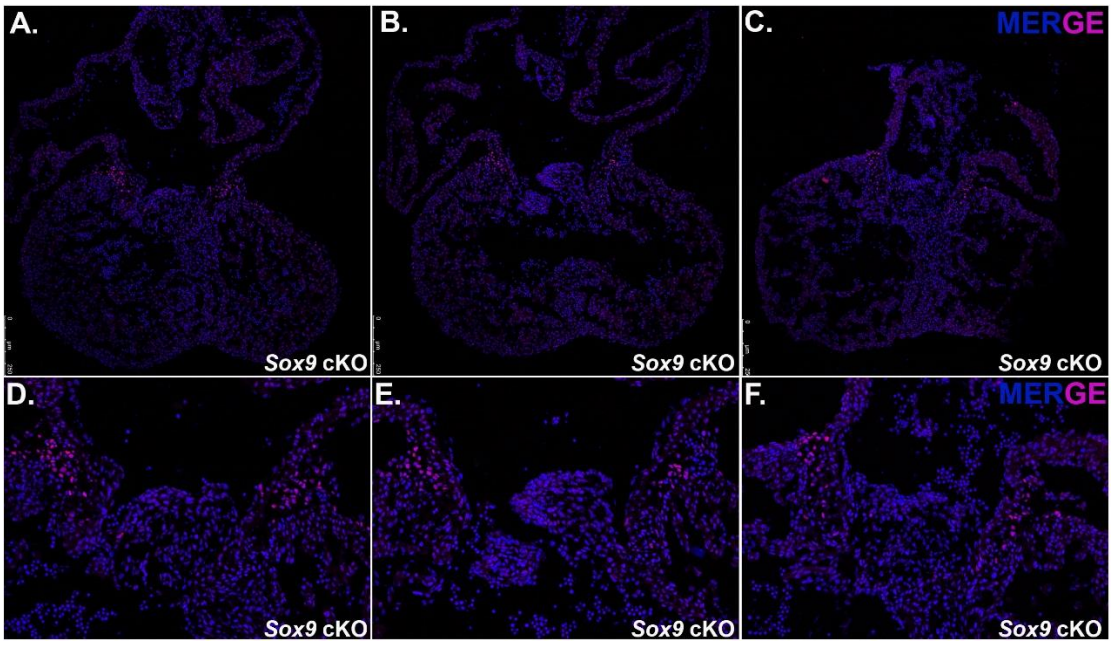

Fig.S4 The loss of SOX9 in multiple E12.5 *Sox9* cKO heart sections. Immunofluorescence for SOX9 merged with DAPI on E12.5 *Sox9* cKO hearts. **A.-C.** Illustrates heart sections from two different *Sox9* cKO hearts. **A., D.,** A separate cross-section from the same *Sox9* cKO heart as in Fig.S3. **B., C., E., F.,** Cross-sections from another *Sox9* cKO heart. **D.-F**. Zoomed in images of the AVC taken from images in **A.-C.** n=2.

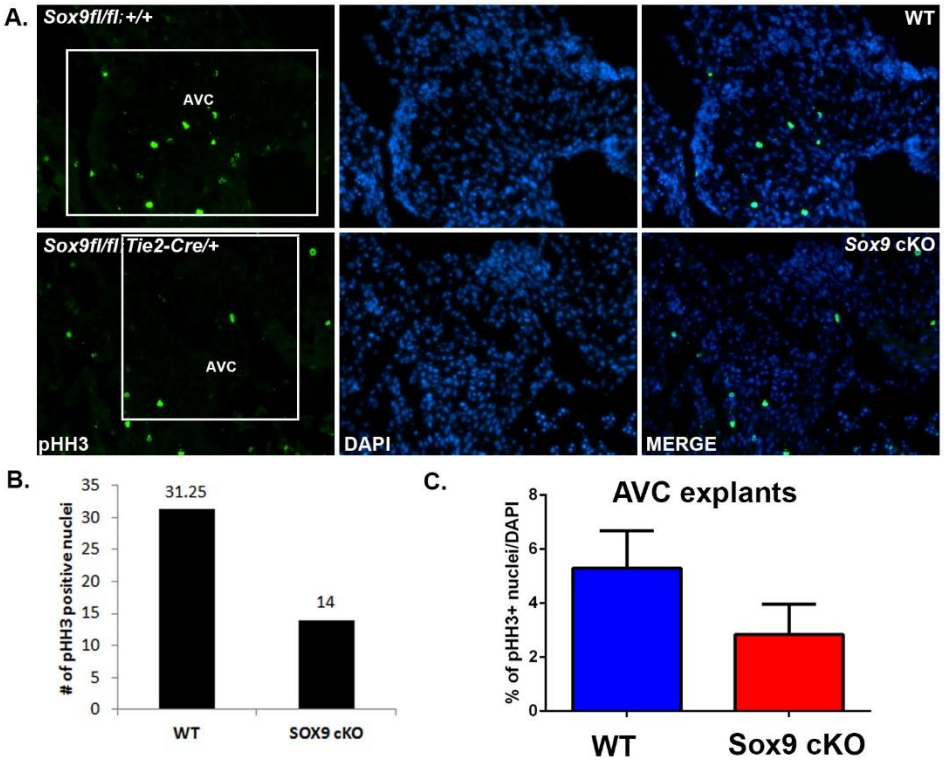

Fig. S5 Reduced proliferation in the *Sox9* cKO AVC. A. Immunofluorescence for phospho histone H3 (pHH3) on E12.5 WT and *Sox9* cKO hearts. Top panel shows *Sox9fl/fl;+/+* (WT) and bottom panel shows reduced proliferation in *Sox9fl/fl;Tie2-Cre* (*Sox9* cKO). Box indicates AVC region used for quantitative assessment. **B.** Counts of pHH3 positive nuclei in the AVC region on WT and *Sox9* cKO hearts. 5 random fields of view were counted in the AVC region from at least 3 mice for each genotype. **C.** pHH3 counts over DAPI counts on AVC explants after culture from E10.5 WT and *Sox9* cKO hearts. Error bars represent standard deviation (SD). N refers to the number of explants taken from different mice. n=7 for WT and n=4 for *Sox9* cKO. The myocardium was excluded from the analysis.

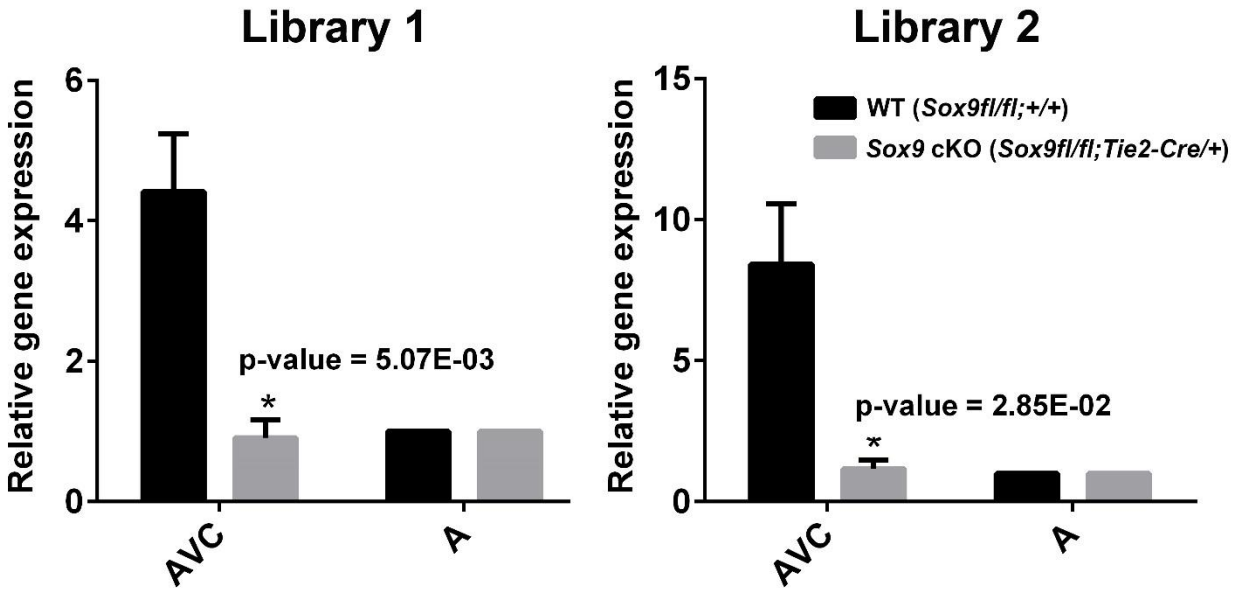

Fig.S6 Significant loss of *Sox9* expression is shown in the E12.5 *Sox9* cKO AVC. Taqman assays for *Sox9* relative to *Gapdh* on 2-3 pooled embryonic valves of E12.5 *Sox9fl/fl* (WT) and *Sox9fl/fl;Tie2-Cre* (*Sox9* cKO) AVC and atria (A). These exact samples were used for each respective RNA-Seq library. This demonstrates that loss of *Sox9* is specific and efficient in the *Sox9* cKO AVC. P-value is determined by a Student's T-test between WT and *Sox9* cKO AVC. Error bars are standard mean error (SEM).

Potential SOX9 sites are red. Mutated sequences are in green.

Normal

>*Mecom* enhancer

TTCAGAAGGTTCTAGAAGCAAGGCACTAGTGTCTGATTTTAAAATGTTGATGGATGTGCATTCCACCCATGTGTAAT
CCCAAATGACAATATGTTTTGTGTCCAGGGCATGCTTCTGACTAAATCAATAACCACCCTAAGTCTGATAAAAGTT
TTACAAAATATCCAAGACATTTAGAGTAATTGTTAACATCTGCTCATTATGATTCAAATGTGTAAGCAGGTTTAGCA
GCCAGATAAATATATTTATTCATCAGCAGCCAGCATGTCACTACTGCCTCAGTGGTGACATAAAACAGTAAGACATT
AGGATTTGCCCGAGTATTGGATTCAGAGAATACAAAGAACCATTGTACAGTGTGTGTGTGGGGGGGGGACAGAAAA
TTCTGATTTCTCCATGTTTTCAGAGACAGAGACAGAGTGGAGGGGAGAAGAGGAAAGAGAAGGGACAAACTTTAGT

Mutate the potential SOX9 dimer site only.

>Mecom SOX9 DM enhancer

TTCAGAAGGTTCTAGAAGCAAGGCACTAGTGTCTGATTTTAAAATGTTGATGGATGTGCATTCCACCCATGTGTAAT
CCCAAATGACAATATGTTTTGTGTCCAGGGCATGCTTCTGACTAAATCAATAACCACCCTAAGTCTGATAAAAGTT
TTACAAAATATCCAAGACATTTAGAGTAATTGTTAACATCTGCTCATTATGATTCAAATGTGTAAGCAGGTTTAGCA
GCCAGATAAATATATTTATTCATCAGCAGCCAGCATGTCACTACTGCCTCAGTGGTGACATAAAACAGTAAGACATT
AGGATTTGCCCGAGTATTGGATTCAGAGAATAGCGAAGAACCAGGTTACAGTGTGTGTGTGGGGGGGGGACAGAAAA
TTCTGATTTCTCCATGTTTTCAGAGACAGAGACAGAGTGGAGGGGAGAAGAGGAAAGAGAAGGGACAAACTTTAGT

>Mecom SOX9 allM enhancer

TTCAGAAGGTTCTAGAAGCAAGGCACTAGTGTCTGATTTTAAAATGTTGATGGATGTGCATTCCACCCATGTGTAAT
CCCAAATGAGCGTATGTTTTGTGTCCAGGGCATGCTTCTGACTAAATGCGTAACCACCCTAAGTCTGATAAAAGTT
TTACAAAATATCCAAGACATTTAGAGTAAGGTTTAACATCTGCTCATTATGATTCAAATGTGTAAGCAGGTTTAGCA
GCCAGATAAATATATTTATTCATCAGCAGCCAGCATGTCACTACTGCCTCAGTGGTGACATAAAACAGTAAGACATT
AGGATTTGCCCGAGTATTGGATTCAGAGAATAGCGAAGAACCAGGTTACAGTGTGTGTGTGGGGGGGGGACAGAAAA
TTCTGATTTCTCCATGTTTTCAGAGACAGAGACAGAGTGGAGGGGAGAAGAGGAAAGAGAAGGGACAAACTTTAGT

Fig.S7 *Mecom* mutant enhancer sequences. DNA sequences for the *Mecom* enhancer and positions of sequence mutations in the *Mecom* enhancer for the SOX9 dimer motif mutant (DM) and all SOX9 motifs mutated (allM). Mutated sequences were generated by Integrated DNA Technologies (IDT) using gBlocks Gene Fragments. Sequences in red represent potential SOX9 motifs. Mutated sequences are represented in green.

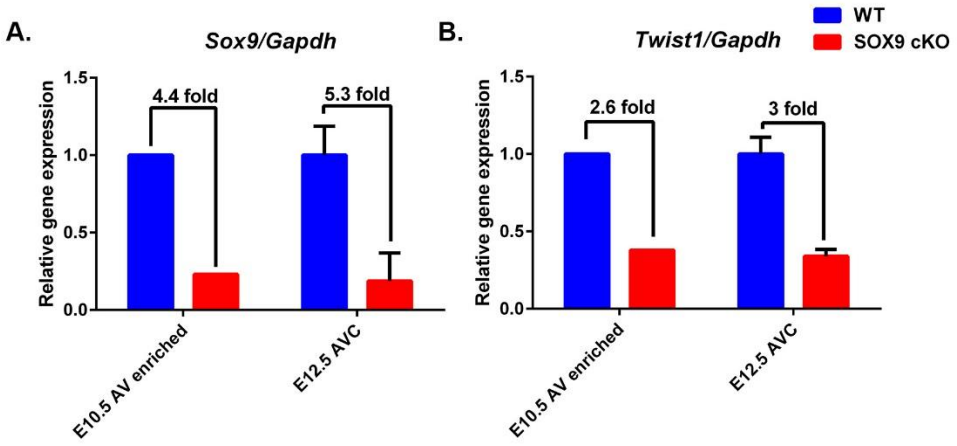

Fig.S8 *Twist1* mRNA expression is reduced in the *Sox9* cKO AVC. Taqman qRT-PCR assays for **A.** *Sox9* and **B.***Twist1* relative to *Gapdh* on E10.5 AV-enriched regions and E12.5 AVC *Sox9fl/fl* (WT) and *Sox9fl/fl;Tie2-Cre* (*Sox9* cKO). Error bars are standard mean error (SEM). At E10.5, n= 2 for WT and n=-1 for *Sox9* cKO, and n=>8 for E12.5.

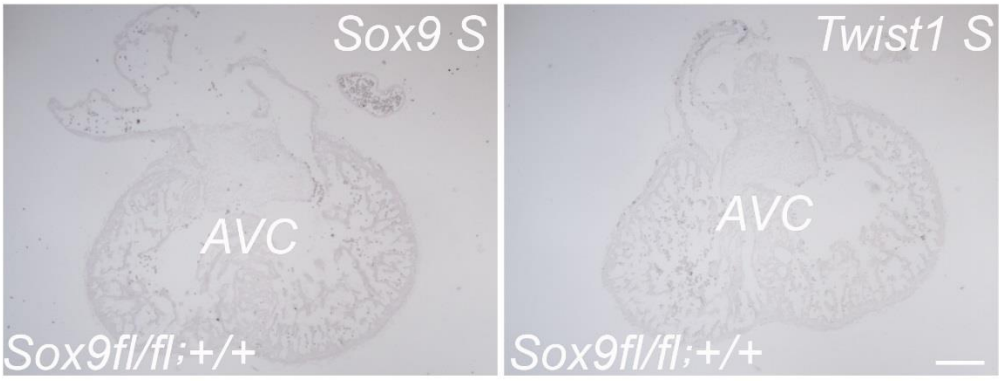

Fig.S9 *Sox9* and *Twist1* DIG-labeled probes are specific. *In situ* hybridization using the sense DIG-labelled probes (S) for *Sox9* and *Twist1* on E12.5 *Sox9fl/fl;*+/+ (WT) hearts to illustrate that antisense staining is specific and not background staining. N=3. All probes on all hearts were stained simultaneously and stopped concurrently. Images were taken at the same exposure.

Supplemental Table List

Table S1: Primers
Table S2: Characteristics of the SOX9 ChIP-Seq libraries
Table S3: E12.5 AVC SOX9 ChIP-Seq peak coordinates and gene associations
Table S4: E12.5 Limb SOX9 ChIP-Seq peak coordinates and gene associations
Table S5: SOX9 monomer and dimer binding sites under the SOX9 peaks in heart and limb
Table S6: SOX9 peak regions that overlap in the E12.5 AVC, limb, and HFSC ChIP-Seq libraries
Table S7: GO analysis using Ingenuity Pathway Analysis on 293 shared SOX9 target genes
Table S8: Genes associated with SOX9 peaks in all three libraries found in the proliferation of cells GO category
Table S9: GO analysis on AVC, limb and HF-SC specific SOX9 peaks to identify unique GO terms and functions
Table S10: RNA-Seq library stats from Tophat2
Table S11: RNA-Seq gene list with ≥0.5FPKM in WT or *Sox9* cKO
Table S12: Genes with +/-1.5 fold change in the *Sox9* cKO with restrictions (≥ 0.5FPKM in either WT or *Sox9* cKO) that also have an associated SOX9 peak

Click here to Download Tables S1-S12